PENNING IONIZATION OF SMALL MOLECULES BY METASTABLE NEON

by

Joseph H. Noroski

B.S., University of Pittsburgh, 1993

M.S., University of Pittsburgh, 2001

Submitted to the Graduate Faculty of

Arts and Sciences in partial fulfillment

of the requirements for the degree of

Master of Science

University of Pittsburgh

2007

UNIVERSITY OF PITTSBURGH

COLLEGE OF ARTS AND SCIENCES

This thesis was presented

by

Joseph H. Noroski

It was defended on

March 23, 2007

and approved by

Kenneth Jordan, Professor, Chemistry

David Pratt, Professor, Chemistry

Thesis Director: Peter E. Siska, Professor, Chemistry

PENNING IONIZATION OF SMALL MOLECULES BY METASTABLE NEON

Joseph H. Noroski, M.S.

University of Pittsburgh, 2007

Penning ionization electron spectroscopy (PIES) in crossed, supersonic molecular beams was used to examine the reactions of Ne* ($2p^5 3s\ ^3P_2$, $^3P_0$) with two target molecules, CO_2 and C_2H_2. Tentative peak assignments were made for each reaction, and the collision dynamics of these reactions were also examined at various collision energies in light of the two potential model of Penning ionization. The 2.6 − 3.2 eV region of the Ne* + CO_2 spectrum is assigned to a nv_1 progression. The region from 2.6 − 2.0 eV is more complex, but a $nv_1 + 2v_3$ progression in addition to the nv_1 progression is very likely present. The region below 2.0 eV contains a broad band of signal, but no assignments have yet been made on this region. The Ne* + C_2H_2 spectrum has a very well resolved v_2 progression around 5 eV. The *A* state of the Ne* + C_2H_2 PIES spectrum is present, but it can't be resolved with our data. The Ne* + CO_2 reaction was run at collision energies of 1.73, 1.97, 2.56, and 3.13 kcal/mol. A red shift (~ −18 meV) was found for all but the 3.13 kcal/mol energy, which was blue shifted (~ 18 meV). This small shift, combined with broad peakshapes, indicates that ionization occurs over the positive and negative regions of the Ne* + CO_2 potential energy surface, that is, ionization straddles the zero-crossing point. The Ne* + C_2H_2 reaction was run at collision energies of 1.80, 2.37, and 2.94 kcal/mol. A decreasing blue shift with increasing collision energy was found (~ 60, 50, and 45 meV,

respectively). Decreasing blue shift with increasing E is not typical and could be due to changing dynamic factors as E increases. Since the shift is significantly smaller for Ne* + CO_2 than for Ne* + C_2H_2, we propose that the interaction between Ne* and CO_2 is less repulsive than that of Ne* and C_2H_2 in the range of geometries over which ionization occurs.

TABLE OF CONTENTS

LIST OF TABLES

LIST OF FIGURES

1.0 PENNING IONIZATION

1.1 PREVIOUS RESEARCH

Penning ionization (PI) can be represented by $A^* + B \rightarrow A + B^+ + e^-$. A* is usually a metastable atom but, sometimes, it is a molecule. A* is produced by bombarding A with an electron beam. The Siska group is primarily interested in the reactions for which the metastable atom is a noble gas. B is the target molecule of our choice. Cermak and Herman[1] (1965) were among the first to suggest determining the kinetic energy of the electrons that are ejected via PI as a means of monitoring gas phase reactions. This type of experiment is dubbed Penning ionization electron spectroscopy (PIES).

PIES experiments involving Ne* were first done, of course, with simple target molecules[2]: He*, Li, Na, Ar, K, Kr, Xe, Cs, and H_2. Many of these experiments were performed in the 1980's. Progress in this field, particularly with Ne*, has been slow for three main reasons. First, the number of scientists initially in this area was small and reduced funding has made that number even smaller. Clearly, pragmatic concerns influence greatly the direction of scientific research. Second, the assignment of peaks becomes much more difficult as the number of atoms in the target molecule increases since there are more molecular orbitals (MO's) from which electrons can be ejected and there are more normal modes of vibration that can be excited. Any

mixing of these normal modes complicates the electron spectrum even more. Third, Ne* does not "pack the same punch" as He*, preventing Ne* from probing as deeply into the innards of target molecules and from ejecting high kinetic energy electrons, which are easier to detect since they are far from the noise prevalent at low kinetic energy. See Table 1.

Table 1: Metastable gas atom characteristics[3]

Atom	Electron Configuration	State	Excitation Energy (eV)
He	$1s2s$	$2\,^1S_0$	20.6158
		$2\,^3S_1$	19.8196
Ne	$2p^5 3s$	$3\,^3P_0$	16.7154
		$3\,^3P_2$	16.6191

Nonetheless, some wayward, yet intrepid, physical chemists persist in this area. B. Lescop *et al.*[4] (1998) examined the PI of CO_2 by Ne*, made peak assignments, and proposed a non-van der Waals interaction between the colliding species. Maruyama[5] *et al*. (2000) examined the PI of CO_2 clusters by Ne*. Additionally, the B. Lescop and F. Tuffin group has explored[6,7,8,9,10] via PIES the reactions of Ne* with NH_3, C_2H_2, H_2O, N_2, and CO. By comparison to NeI photoionization the NH_3 results showed that Ne*/NH_3 interaction influences the ionization dynamics and, in typical fashion, they explored the agreement of vibrational populations with Franck-Condon factors. Vecchiocattivi (1990) *et al.*[11] have also conducted crossed beam studies of excited neon on many small molecules to determine total ionization cross sections. Only recently has the Vecchiocattivi group configured their apparatus to perform

kinetic energy studies in the manner that P. E. Siska mastered in ages past. See below. In a study[12] (2005) of the Ne* + N_2O reaction, the Vecchiocattivi group explored the products of autoionization via mass spectrometry as well as the correlation between the collision energy and the molecular orbitals of N_2O that are involved in the process. A follow up paper[13] (2005) contains a theoretical investigation of this same reaction with the finding that "orientation effects tend to become less pronounced with increasing collision energy."

Over the past decade, the Siska group has explored He* reactions[14,15,16] with H_2, HD, D_2, N_2, and CO and those of Ne* with H_2[17], NO[18], and CO_2. Since the accepted mechanism for PI involves the transfer of a valence electron of B into the "hole" in the core of A*, the study of He* ($2\ ^1S_0$, $2\ ^3S_1$) was the logical place for all research in this area to begin since the collisions involve spherically symmetric *s* orbitals. A once-proposed competing mechanism, the radiative mechanism, supposes that the metastable relaxes and emits a photon, which ionizes the target molecule. The relatively long lifetime of the metastable at supersonic beam conditions, however, essentially eliminates the possibility of this mechanism.[19] The reactions with Ne*, however, are significantly more complicated. The metastable states possess angular momentum ($^3P_{2,0}$), and the hole in Ne* is in a *p* orbital, leading to geometrically dependent collisions. How these differences affect PI reactions are still unsettled questions. Further, the smaller energies involved are more likely to produce states that are resonant with a densely packed set of states known as Rydberg states, which exist in the continuum of states for the $A + B^+ + e^-$ system and result from weakly held electrons (see below). While laying the groundwork for serious research into these Rydberg states, our recent efforts mainly have been focused on determining the kinetic energy dependence of the Ne* PIE spectra that have been obtained over the recent years by

various undergraduate and graduate researchers. Confirmation of Lescop's assignment of the vibrational progressions that are excited by the reaction of CO_2 with Ne* is also a goal. For the sake of reference and discussion in this thesis, we include the ground state valence electron configurations, term symbols, and point groups of the molecules of recent interest to our group:

CO_2: $(1\sigma_g)^2(1\sigma_u)^2(2\sigma_g)^2(2\sigma_u)^2(1\pi_u)^4(1\pi_g)^4$ $^1\Sigma_g^+$ $D_{\infty h}$

C_2H_2: $(1\sigma_g)^2(1\sigma_u)^2(2\sigma_g)^2(2\sigma_u)^2(3\sigma_g)^2(1\pi_u)^4$ $^1\Sigma_g^+$ $D_{\infty h}$

N_2O: $(4\sigma)^2(5\sigma)^2(6\sigma)^2(1\pi)^4(7\sigma)^2(2\pi)^4$ $^1\Sigma^+$ $C_{\infty v}$

We could have included "+" notation with the sigma orbitals, such as $1\sigma_g^+$, since these are linear molecules and the MO's that are cut in half by a mirror plane that contains the bond axis do not change sign upon reflection.

1.2 THE TWO POTENTIAL MODEL

The "kinetic energy" of which we spoke above is the initial, relative kinetic energy, based on the *relative* velocity $\boldsymbol{v}_{rel}$ of the two soon-to-be-colliding reactants, which approach each other in a crossed beams manner. See Figure 1.

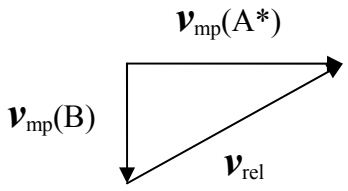

Figure 1: The relative velocity vector diagram for a crossed beams experiment. $\boldsymbol{v}_{rel}$ is given by $\boldsymbol{v}_{rel} = \boldsymbol{v}_{mp}(A^*) - \boldsymbol{v}_{mp}(B)$ in order to abide by the convention that $\boldsymbol{v}_{rel}$ should point in the direction of the atomic beam in an atom-molecule system. $\boldsymbol{v}_{mp}$ is the most probable velocity of gas particle A or B. The calculation of $\boldsymbol{v}_{mp}$ is shown in detail in the Appendix.

Others refer to the relative velocity as the *asymptotic* velocity, referring to the flat part of the A* + B potential curve ($R \rightarrow \infty$) shown in Figure 2, which illustrates the classical interpretation of PI, the "two potential model" potential energy diagram. With μ as the reduced mass, we define this relative kinetic energy as the *initial energy of the system*, E:

$$E = \frac{1}{2}\mu v_{rel}^2 \tag{1}$$

E is the total energy, *excluding excitation of* A*, of the A* + B system, and it remains constant throughout the reaction. (Figure 2 clearly shows that the excitation energy of A is not included in E.) To conduct kinetic energy dependence studies, we heat the less massive reactant. [Ohno attempts to perform kinetic energy studies, using time of flight methods[20,21]. We feel that this method, which uses pulses of metastable beams with a Maxwellian distribution, does not provide a definite kinetic energy. This is due to fast metastables at the back end of the pulse colliding with slower metastables at the front of the pulse, which transfers energy to the slower metastables and clouds the energy distribution that we calculate from the velocities of the

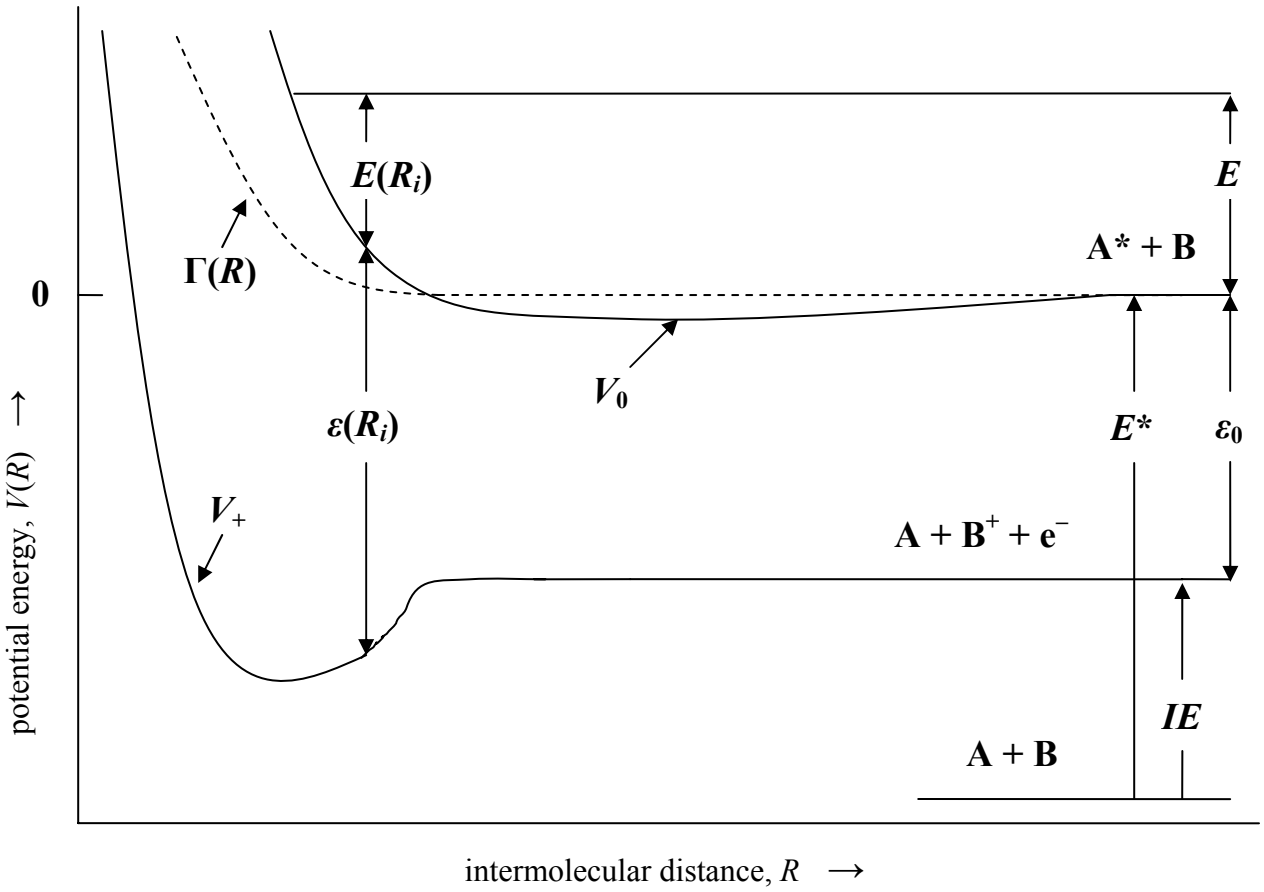

Figure 2: The two potential model for PI. The flat region ($R \rightarrow \infty$) of V_+ is exaggerated to aid in visualization of the importance of the difference $\varepsilon(R_i) - \varepsilon_0$ to our extraction of dynamical information from PIES experiments. The appearance of the well in V_+ in the actual case is not so sudden.

metastables. The Ohno group describes this as two-dimensional PIES. The two dimensions are the ejected electron kinetic energy and the kinetic energy dependence.] This produces a larger change in E than heating the more massive reactant because less massive objects move faster, via KMT, and E is proportional to the square of the relative velocity. The information that we learn from kinetic energy studies is *dynamical* information, where dynamics refers to the *forces* at work during the collision event. The forces, of course, can be repulsive or attractive. Whether the electron ejection occurs while the interaction between the colliding species is attractive or repulsive is determined by the deviation of the energy $\varepsilon(R_i)$ from ε_0. See Figure 2. $\varepsilon(R_i)$ is the kinetic energy of the electrons that are ejected during a PIES experiment and, therefore, equals the difference in energy between the A* + B and the $A + B^+ + e^-$ potential energy curves (V_0 and V_+, respectively) at the distance where electron ejection occurs, R_i. ε_0 is the difference between the excitation energy E^* of A* and the ionization potential IE of B: $\varepsilon_0 = E^*(A^*) - IE(B)$. In other words, ε_0 is the kinetic energy of ejected electrons that our PIES experiment would yield if the electron ejection could be made to occur at infinite separation, that is, a process based purely on orbital energies. Of course, electrons never decide to jump that far. They act when compelled to do so by the forces at work when the donor and acceptor orbitals of the reactants are in close proximity. If reaction occurs, then, $\varepsilon(R_i)$ will differ from ε_0 because the potential energy curves of the reactants and products are not straight lines; *the colliding reactants interact*.

One can view the upper curve (V_0) as being "correct" or "in operation" from large R up until the point of electron ejection, that is, on the incoming trajectory. At $R = R_i$ the bottom curve "turns on" and becomes the "correct" indicator of the potential energy situation for whatever species are formed from the collision. For our model the V_+ curve describes the

products $A + B^+ + e^-$ on their journey away from the collision, the outward trajectory. Other products are possible and result from associative, dissociative, and rearrangement ionization. If, for example, the product $[AB]^+$ forms during the reaction, it can be trapped in the potential well of V_+. This would not, however, affect the kinetic energy of the ejected electron that is measured in the PIES experiment. Note that the irreversible, vertical $\varepsilon(R_i)$ transition of Figure 2 can occur from two different regions of the upper curve – the attractive well, where $V_0 < 0$, or the repulsive region, where $V_0 > 0$. The point where a potential curve (e.g., V_0 or V_+) changes sign is called the zero-crossing point. Ionization over the attractive well yields $\varepsilon(R_i) < \varepsilon_0$. (Note that since there is a well, it is possible that several values of R can yield ejected electrons of the same kinetic energy.) When the actual kinetic energy of the electron, $\varepsilon(R_i)$, is less than the prediction based solely on orbital energies, ε_0, scientists say that the transition is "shifted to the red". Ionization over the repulsive region gives $\varepsilon(R_i) > \varepsilon_0$, and the transition is "shifted to the blue". It is crucial to note that this qualitative shift idea, ε_0 versus $\varepsilon(R_i)$, which is necessary if we are to explain PIES in any simple manner, depends on the approximation that V_+ is nearly flat up until the point of electron ejection. This approximation is bolstered by the fact that A* has a very large radius, which induces a repulsive interaction between A* and B at much larger R than the R at which A and B^+ experience repulsion. Thus, the crossing point of V_0 occurs earlier in the collision than does the crossing point for V_+. The red shift/blue shift concept requires that the total collision energy E, as defined above, be conserved for the entire process. An attractive interaction between A* and B accelerates the reactants toward each other, increasing their kinetic energy. If electron ejection occurs at this point, the ejected electron must carry away less energy than ε_0. A repulsive interaction between A* and B causes the reactants to slow down as they approach. If

electron ejection occurs at this point, the ejected electron must carry away more energy than ε_0. We can express this relationship mathematically as follows:

$$E = V_0(R_i) + E(R_i) = V_+(R_i) + E'(R_i) + \varepsilon(R_i) \tag{2}$$

$E(R_i)$ is the reactants' kinetic energy at R_i, $E'(R_i)$ is the products' kinetic energy, and $\varepsilon(R_i)$ = $V_0(R_i) - V_+(R_i)$. In general $E(R)$ is the classical, local, heavy-particle kinetic energy, including centrifugal energy, and $E(R)$ is proportional to the square of the local, relative velocity of the particles. In attractive interactions, the relative velocity of the reactants increases as the collision occurs, increasing $E(R)$. In repulsive interactions, the relative velocity of the reactants decreases as the collision occurs, decreasing $E(R)$. $E(R)$ is not directly measurable. The interplay between $E(R)$, E, and V_0 is reflected in the upper curve of Figure 2. An experiment at only one temperature provides red shift or blue shift information for that E alone. By performing the experiment at different temperatures, we can monitor how an increase in E affects the kinetic energy of the ejected electron, that is, monitor the change in the magnitude of the red or blue shift, and gain information about the shape of the upper curve (A* + B) up to the point of electron transfer. Repulsive interactions are the most common type, and the A* + B potential energy curves often have shallow wells. Attraction can be found in cases where the target molecules have unpaired electrons and spin states which allow for electron transfer.

The resonance width $\Gamma(R)$, which has the unit of energy, is the first quantity in Figure 2 that takes us way beyond (even for thoughtful chemistry neophytes) the easy to grasp (classical!) concepts represented by the other symbols because it is closely related to Fermi's Golden Rule.

Namely, $\Gamma(R) = 2\pi\rho_\varepsilon \left| V_{0\varepsilon}(R) \right|^2$. Stated in this form, $\Gamma(R)$ can be understood in terms of the mechanism described by Miller[22] in his nearly biblical paper. Now, the lower curve in Figure 2 represents *a single state* of the $(A\text{-}B)^+ + e^-$ system, which dissociates to ground state A and ground state B^+. In fact, this curve is the lower bound of a *continuum* of states of this system. What leads to the continuum? The ejected electron is not bound, and, therefore, its energy is not quantized, so the energy between V_0 and V_+ is continuously variable, leading to a continuum of states. For this reason Miller describes PI as the "leakage" (i.e., transition) from the discrete state found on the V_0 curve to a state in the continuum that is degenerate with it. These suppositions are represented in our Γ equation where ρ_ε is the density of states in the continuum and $V_{0\varepsilon}(R)$ is the coupling (i.e., an integral that must be evaluated) between the discrete and continuum states. The stronger the coupling, the more likely it is that a transition will occur. (More precisely, $V_{0\varepsilon}(R)$ is the transition matrix element between the two states involved in the transition, and, when appropriate wave functions are used, the resonance width is expressed as $\Gamma(R) = 2\pi \left| V_{0\varepsilon}(R) \right|^2$.) The proper description for $\Gamma(R)$ and $V_{0\varepsilon}(R)$ is found elsewhere[22][23], but a further qualitative description of $\Gamma(R)$ can be found below.

In addition to dynamical information, PIES yields information about the population of the electronic and vibrational levels of the dawning Penning ions (not the neutral target molecule). Since the electrons produced in PIES are ejected essentially instantaneously, the electrons provide us "real time" or "snap shot"-like information about which electronic and vibrational levels are occupied. This is, of course, the general situation that we find in photoelectron spectroscopy. For emission from non-bonding or weakly bonding or weakly anti-bonding MO's, we expect that the nuclear arrangement of the ion will be very similar to that of the neutral

molecule. This leads to strong overlap of the $\upsilon = 0$ and $\upsilon' = 0$ vibrational levels in a Franck-Condon sense, indicating that vibrational excitations are weak and long vibrational progressions will not be seen. Conversely, emission of an electron from a strongly bonding or strongly anti-bonding MO should result in significant nuclear rearrangement. Therefore, the upper potential well will be shifted to a longer or shorter r_e, respectively. This leads to *vertical transitions* that are stronger for $\upsilon = 0$ to $\upsilon' \neq 0$, implying that a significant vibrational progression will be evident. The $\upsilon = 0$ to $\upsilon' = 0$ transition above is called the *adiabatic transition*, and Table 2 contains a brief list of adiabatic ionization potentials, the energy required to produce such a transition, for molecules that we are currently investigating in the Siska group: H_2, CO_2, N_2O, and C_2H_2. Note that such a simple description as a $\upsilon = 0$ to $\upsilon' = 0$ transition only applies to a molecule, such as hydrogen, with one normal mode of vibration. The H_2 ionization spectrum is simplified even further because it has only one occupied MO. CO_2, however, has four normal modes of vibration, two of which are degenerate, and eight occupied valence MO's. Thus, an "adiabatic transition" can occur from each occupied MO of CO_2. Ionization of the HOMO ($1\pi_g$) gives the so-called *X* state. Ionization of the next highest-lying MO ($1\pi_u$) gives the *A* state. Next is the *B* state, then the *C* state, and so on. Now, for example, within the *X* state any of the three energetically distinct normal modes can be excited, and it makes no sense to discuss a $\upsilon = 0$ to $\upsilon' = 0$ transition. The only correct way to indicate the adiabatic transition for the *X* state of CO_2 is $(000)\,^2\Pi_{g,3/2} \leftarrow (000)\,^1\Sigma_g^+$. The set of zeros ($\upsilon_1\upsilon_2\upsilon_3$) indicates the vibrational modes, the symmetric stretch (υ_1), the (doubly degenerate) bend (υ_2), and the antisymmetric stretch (υ_3). In C_2H_2 there are seven normal modes and, for example, the adiabatic transition for the *X* state is written as $[00000]\,^2A_g \leftarrow [00000]\,^1\Sigma_g^+$. υ_1 is C−H symmetric stretching, υ_2 is C−C symmetric stretching, υ_3 is C−H asymmetric stretching, υ_4 and υ_5 are doubly degenerate bending modes.

Thus, an adiabatic transition occurs when a molecule that is in its vibrational ground state, that is*, all normal modes are in the ground state*, is ionized into an ionic state (be it *X*, *A*, …) in which *all normal modes are in the ground state*. This is the lowest energy transition (that produces an ion) that can occur within an electronic state, and this energy is traditionally called the "ionization energy" of an orbital. Further, then, this means that all progressions that involve excitation of a single vibrational mode (e.g., $[\upsilon_1 0000] \leftarrow [00000]$, $[0\upsilon_2 000] \leftarrow [00000]$, etc.) must originate from the same energy. In the analysis section of this thesis, peak assignments will be made on the PIES spectra that are based, in part, on excitation of normal modes of vibration. Such a discussion, however, depends on the validity of the Born-Oppenheimer approximation to the particular transition. When this approximation is (nearly) correct, the potential surface of the ion is very similar to that of the neutral molecule, and strong Franck-Condon overlap is expected. As there is with C_2H_2's *A* state, however, there is a change in symmetry, and the $[00000] \leftarrow [00000]$ transition is very difficult to determine precisely.[24] This is explored further below.

2.0 EXPERIMENTAL

2.1 VACUUM SYSTEM

Of course, if we want to examine the reaction of Ne* with CO_2, we must get rid of other gases, so our PIES experiments are performed under high vacuum conditions in a non-magnetic, stainless steel "box". The main chamber has inside dimensions of 32.5" × 31" × 24" and is accessed via a removable 39.5" × 31" × 1.25" aluminum cover, which acts as one of the chamber walls. The main chamber houses the reaction center and the buffer chambers for A* and B. The metastable (A*) beam source is dubbed the primary source, and the target (B) beam source is called the secondary beam source. The primary and secondary beam sources are attached to separate stands with wheels, allowing us to "plug" each beam source into the appropriate buffer chamber. The wheeled stands allow for relatively easy removal of the source chambers for maintenance. An overhead view of the instrument is shown in Figure 3.

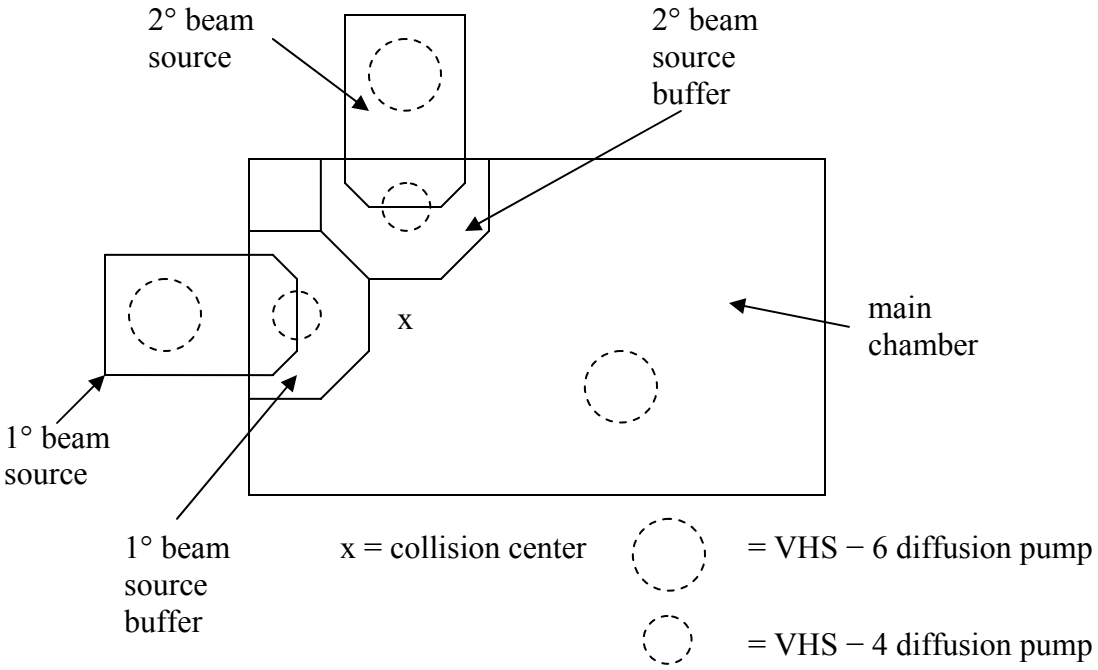

Figure 3: The five regions of our crossed beams PIES instrument.

A high vacuum is obtained by first pumping each chamber with *mechanical pumps*. The main and secondary (source and buffer) chambers are pumped with Alcatel direct drive (no belts) mechanical pumps (Model 2033 and 2033C, respectively). The secondary pump's parts are Teflon coated to resist chemicals, allowing us to examine radicals such as NO or other nasty molecules. The primary chamber (source and buffer) is first pumped with a Welch Duo-Seal Vacuum Pump (Model 1397). Two smaller Alcatel pumps (M2004A) are used to pump out the HeI lamp, the primary and secondary gas manifolds, and the quench lamp, which is part of the electron gun. Once the mechanical pumps have reduced the pressure to 0.1 torr, bellows are used to close them off from the respective region, allowing us to open all five regions to *diffusion pumps* (dp's) (Varian VHS − 6 and VHS − 4 models) via gate valves. The mechanical pumps remain open to the dp's as the dp's operate. These dp's operate by vaporizing silicon oil and cooling the vapor as it rises. As the cooled oil sinks back into the dp, it draws gaseous particles down with it, creating a better vacuum. Ultimately, we achieve a pressure of roughly 3×10^{-7} torr in the main chamber and pressures of roughly 5×10^{-8} torr in the primary and secondary chambers.

2.2 GAS INTRODUCTION

Figure 3 shows that the reactants are shot at reach other at a right angle – a so-called "crossed beams" experiment. The beams are supersonic and have high centerline intensity, narrow velocity distribution, and high number density. This type of beam is produced, as opposed to a simple effusive beam, through the use of a gas nozzle with a 76 μm diameter orifice. This

"bottleneck" produces pressures on the order of several thousand torr and, therefore, many collisions that virtually eliminate any velocity component that is perpendicular to the beam of gas. Stated simply, the high number density allows for many collisions and a large number of ejected electrons, *which is our signal*. This is a common sense idea. A narrow velocity distribution, however, helps us in a more sublime way. Referring to Figure 2, you will note that E is drawn as a sharp line. Is this possible? Let us begin by imagining that we could create collisions of identical E by having identical velocities for each reactant. Even at this hypothetical, infinitely sharp E, transitions can still, theoretically, occur at *any* R between the turning point and large R, because the transition process is governed by the quantum mechanical quantity $\Gamma(R)$. $\Gamma(R)$ becomes significant, however, only at smaller R. Concomitantly, the probability that a reaction will occur becomes significant only at smaller R. Thus, the quantum nature of $\Gamma(R)$ dictates that ***identical*** *transitions occur over a small* ***range*** *of R values around* R_i. (Recall that all things in quantum mechanics are "fuzzy" due to Mr. Werner H.) Now, let's allow E to cover a small range of values, as it does in the actual case with a real velocity distribution, meaning that there is now a spread in the turning points for the various E's. For example, the largest E in the distribution has the turning point of smallest R. This spread in E, coupled with the increase of $\Gamma(R)$, enlarges further the range of R values for which ***identical*** *transitions* can occur. From Figure 2 transitions at different R_i's give different $\varepsilon(R_i)$'s which we record as peak broadening. Thus, more definite E's produce sharper peaks, justifying the use of supersonic nozzles. In addition to producing the supersonic beams, these nozzles can be heated (with wire-wound ceramic rods that surround it) or cooled (by sending liquid nitrogen through the water cooling lines) to generate beams at different temperatures, allowing us to conduct

experiments at different kinetic energies E. Further, we eliminate (we hope) any Doppler broadening by having the axis of the lens entrance positioned 90° from the collision plane.

The primary beam source's electron gun, which we noted above was the means to excite A to A*, is designed to excite, in our case, noble gases via a head on collision. This produces in the case of helium two metastable states: He*($1s2s\ ^1S_0$) and He*($1s2s\ ^3S_0$). For all of the other noble gases, we get $^3P_{0,2}$ states from electron configurations $np^5\ (n + 1)s$. In particular, and more explicitly, we get the following for neon: Ne*($2p^5 3s\ ^3P_2$) and Ne*($2p^5 3s\ ^3P_0$), with a 3.35 ± 0.20 : 1 $J = 2 : J = 0$ intensity ratio.[25] When resolving peaks, therefore, we must account for peaks due to both states of Ne*. Now, the electron gun produces many excited states, not just the ones shown above. For example, the configuration Ne*($2p^5 3s$) also produces the states $^3P_1$ and $^1P_1$. Why then do we say that only $^3P_2$ and $^3P_0$ are important? $^3P_2$ and $^3P_0$ are *metastable states*, states that are long-lived on a molecular timescale. General selection rules, the rules that must be obeyed for a transition to occur, require that $\Delta J = 0$ or ± 1 (but $J = 0$ to $J = 0$ is forbidden), $\Delta L = 0$ or ± 1 (but $L = 0$ to $L = 0$ is forbidden), and that $\Delta S = 0$. Thus, a transition from any ^3P state to the ground state of neon $^1S_0$ is spin-forbidden because $\Delta S = -1$. Since the $^3P_1$ state is, however, not present in the reaction center it (and certainly other states) must find a way to radiate its energy quickly via an alternate pathway that *is* allowed. The $^1P_1 \rightarrow {}^1S_0$ transition has $\Delta J = -1$, $\Delta L = -1$, and $\Delta S = 0$, indicating that it is fully allowed. The gun also contains an optical absorption lamp that allows us to select the metastable state ("state select") we wish to examine. (The phrase often used for this process is "quenching".) The state selection lamp operates by exciting one metastable atom, the one we wish to remove, further to an electronic state that is not forbidden from relaxing to the ground state, $1s^2\ ^1S_0$. For example, a He resonance (quench) lamp

(20582 Å light) induces the appropriate transitions that remove the $1s^1 2s^1\ ^1S_0$ state, leaving only the $1s^1 2s^1\ ^3S_0$ state.

Additionally, our PIES device has a windowless HeI discharge lamp which is positioned antiparallel to the metastable beam. This high voltage (2.4 kV) lamp is run at a pressure of ~2 torr, and most of the He is pumped away before it reaches the main chamber. The main chamber pressure does, however, rise to about 3×10^{-6} torr when the lamp is in operation. The 584 Å (21.21804 eV) photons that are produced by this lamp are used to calibrate (peak position and transmission of electrons) the instrument through well known photoelectron spectroscopy (PES) data. An example of this is presented in the Results section.

2.3 ANALYZER, LENS, AND MULTIPLIER

The final major component of our spectrometer is the analyzer, the Comstock AC-901 160° electrostatic energy analyzer, and the einzel lens, Comstock model EL-301. Figure 4 shows these crucial parts, which are made from oxygen free copper. A grounded entrance cap performs the first step of the collimation process of the ejected electrons. "Grounded" means that electrons that come into contact with the cap are whisked away, through a conductor, to the earth − the ground! The electrons next encounter the lens, which lies 0.55" above the collision center and is perpendicular to the plane of the molecular beams. The lens, which is a series of three "plates" (hole diameter = 2 mm), captures electrons that wander into its 0.002 sr acceptance angle, accelerating them in order to focus[26] them into the analyzer. The acceleration and

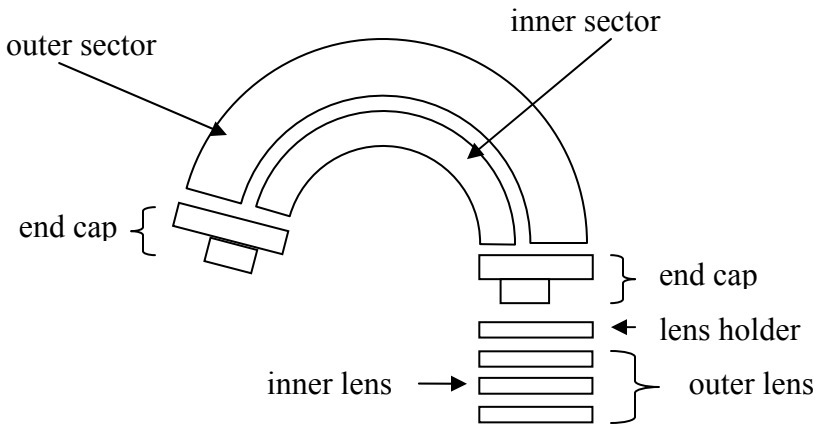

Figure 4: The electrostatic analyzer and einzel lens. Side plates are not shown.

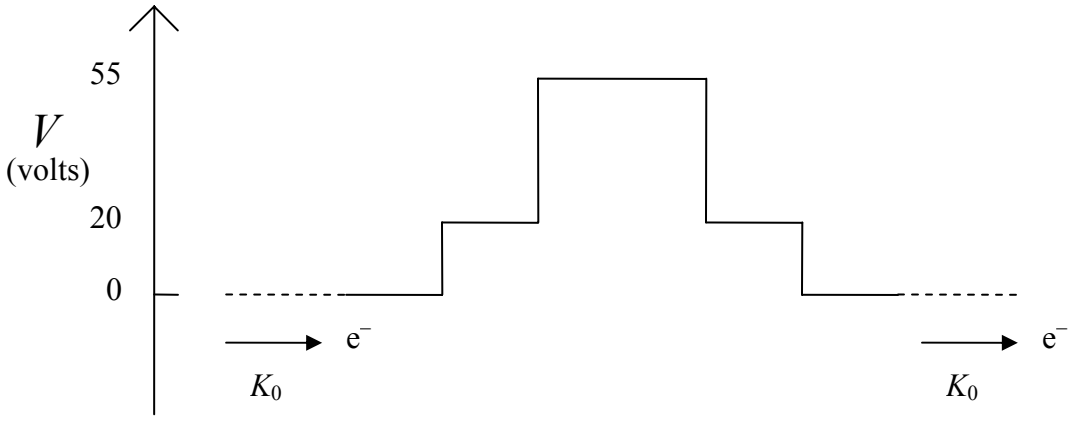

Figure 5: Lens voltages as applied to focus an electron of initial kinetic energy $K_0 = 4.5$ eV. The kinetic energy K at any point along the electron's path can be obtained from the formula $K = K_0 - eV$. K_0 is the kinetic energy of an ejected electron, e is the unit of charge (negative for an electron), and V is the applied voltage. While K will change as the electron travels through the lens, the electron will emerge from the lens with $K = K_0$.

subsequent focusing is achieved by a combination of voltages applied to the inner lens (+55 V) and the outer lens (+20 V). Typical voltages are shown in parentheses. See Figure 5.

After being focused the electrons traverse the sectors and, ultimately, reach the multiplier. This is the physical path of the electrons, but nothing has been said about how we *distinguish* the ejected electrons that have various kinetic energies. To achieve this, first note that we run the experiment at constant pass energy E_p (4.5 eV). "Constant pass energy" means that the *only* electrons that safely pass through the sectors to reach the detector do so with an energy of 4.5 eV. Geometry and applied voltages achieve this according to the equation[27]

$$E_p = \frac{\Delta V}{\left(\frac{r_1}{r_2} - \frac{r_2}{r_1} \right)}. \tag{3}$$

r_1 and r_2 are the radii of the sectors, 4.05 cm and 3.25 cm, respectively. Thus, E_p = 2.254 ΔV. ΔV is the electric potential difference (i.e., voltage) between the outer and inner sectors and equals 1.996 V, achieving a pass energy of 4.5 eV. (The average of the sector potentials is the pass energy.) Electrons that have kinetic energies different than this will be cast headlong into the sectors. As described so far, the only *ejected* electrons that can safely reach the multiplier are those with a kinetic energy of 4.5 eV. This would be a rather useless device. The way we discriminate between electrons of different kinetic energies is by applying a *ramping voltage*, E_V. As an example of how the ramping voltage works, consider the HeI + N_2 experiment, where we scan for photoelectrons with kinetic energies in the range 0 − 6 eV, using a ramping voltage range of +4.5 eV to −1.5 eV. The ramping voltage is slowly added to or

subtracted from (some say "floated on") the initial voltage of the lenses and all of the parts of the analyzer (sectors, end caps, side plates) in small steps (20 meV), maintaining ΔV in Equation 3. At a ramping voltage of +4.5 eV (outer lens at +24.5 V and inner lens at +59.5 V) an electron of 0 eV will be "sucked" into the lens and accelerated to 4.5 eV. When the ramping voltage is at 0 V, electrons of 4.5 eV (if any) that are ejected from the reaction center enter the lens without acceleration or deceleration. In this case, the lens only performs its focusing duties with the lenses at +20 and +55 V. If an electron has a kinetic energy of 6 eV, a ramping voltage of −1.5 V is needed to slow down the electron to 4.5 eV. Thus, the initial lens voltages pull in many electrons of different kinetic energies, but the ramping acts as a filter, allowing only those with kinetic energy of 4.5 eV to reach their destination. A word about units is clearly in order. We appear to be mixing volts, the unit of electric potential, and eV, a unit of energy. Recall, however, that if a *single* electron travels through an electric potential difference of x V, it acquires x eV of kinetic energy. If an electron is ejected with 2 eV, the ramping voltage must supply an additional 2.5 eV of kinetic energy by applying a voltage of 2.5 V to the path that the electron takes. Thus, we can state $\varepsilon(R_i) + E_V = E_p$, and we can view the ramping voltage, E_V, as the energy in eV that the electron acquires or loses due to the applied potential. Note that we have not paid attention to the sign of the voltage.

The multiplier is a K and M Electronics CERAMAX 7551m channel electron multiplier. The most basic possible description of the function of this detector is that the front end of the multiplier, a cone shaped collector, is maintained at ~ +200 V while the back end is maintained at +2.5 kV. This large potential difference encourages the electron cascade in the electron

multiplier. This ends the brief instrument overview that was meant to highlight the key components of our spectrometer that functions as a PES or a PIES device.

3.0 RESULTS AND ANALYSIS

The goal of this present work is to make peak assignments for and preliminary predictions about the dynamics at work in our recent experiments: Ne* + CO_2 and Ne* + C_2H_2. The Ne* + CO_2 reaction was performed at four different collision energies E (i.e., E as defined above): 1.73, 1.97, 2.55, and 3.13 kcal/mol. This was achieved by maintaining the CO_2 beam at 40 °C while heating the Ne* nozzle to 40, 110, 280, and 450 °C, respectively. The Ne* + C_2H_2 experiment was performed at three kinetic energies: 1.80, 2.37, and 2.94 kcal/mol for Ne* nozzle temperatures of 40, 245, and 450 °C. See the Appendix for calculation of these energies. To make peak assignments, a simple energy correction will be made to the raw spectral data of our PIES experiments. From ionization potentials of the appropriate molecular orbital (see Table 2) and the energy of HeI radiation (21.21804 eV), we can determine the theoretical peak positions (i.e., where the peaks *should* be) of the PES spectrum. We assume that the theoretical PES peak positions are immutable at these experimental conditions; the electron energy levels are not altered by the interaction of the HeI photon with the target, CO_2. This is the standard assumption for systems that don't involve excitation from very intense sources (e.g., lasers), where the simultaneous absorption of many photons can lead to significant changes in the electron energy levels (radiation or power broadening[28]). The difference between the theoretical position and the actual position indicates the shift of the entire spectrum, allowing us to apply this difference to all of the peaks in the PIES and PES spectra. This method is much less reliable if there is

Table 2: Adiabatic ionization potentials of some small molecules

Molecule	State	Adiabatic Ionization Potential (eV)
H_2	*X*	15.42593[29]
CO_2	*X*	13.7772[30]
	A	17.3132 (Ref. 30)
	B	18.0761 (Ref. 30)
	C	19.394[31]
N_2O	*X*	12.8898[32]
	A	16.3896[33]
	B	17.65[34]
	C	20.11 (Ref. 34)
C_2H_2	*X*	11.403[35]
	A	16.297 (Ref. 35)
	B	18.391 (Ref. 35)

significant overlap of the PIES and PES peaks. If this is the case, one can seed the target gas with a different noble gas (e.g., Xe), providing well resolved peaks and a reliable shift value. The correction runs as follows. Note first Figure 6, the raw spectrum for the Ne*(40 °C) + CO_2 PIES experiment that was run in conjunction with the HeI + CO_2 PES. The raw data indicates ejected electrons of kinetic energies of 3.75, 3.00, and 1.69 eV for the adiabatic transitions of the *A*, *B*, and *C* states, respectively. The actual values are 3.90, 3.14, and 1.82 eV, values obtained by subtracting the ionization potential of each orbital (Table 2) from 21.21804 eV. The average of the difference is 0.14 eV, and this value is added to each kinetic energy in the raw data for the Ne*(40 °C) + CO_2 PIES experiment, yielding Figure 7. Note that the PES peak energies are very precisely known, but such a large number of significant figures exceeds the number of significant figures that we can obtain with our instrument.

At each temperature the calibration was performed, and the resulting energy correction, as described above, was added to the raw data kinetic energies. Namely, 0.20, 0.21, and 0.22 eV were added to the Ne* + CO_2 raw data for the reactions at 110, 280, and 450 °C, respectively. The result for all four collision energies is shown in Figure 8. Since each spectrum is the result of 40 sweeps, it is readily apparent, assuming no change in instrument performance, that the ionization cross section decreases with increasing *E*. (The ionization cross section is, qualitatively, a measure of the probability of reaction.) This result for CO_2 has been quantitatively determined previously[11]. This decreasing cross section is also the likely culprit for the dramatic disappearance of the broad band of signal between 0.5 and 1.5 eV at the two higher *E* collisions. The assignment of peaks grows in complexity *very* quickly as the number of atoms in the molecule of interest grows. Luckily, Ne* can only ionize CO_2 into the $X\,^2\Pi_g$

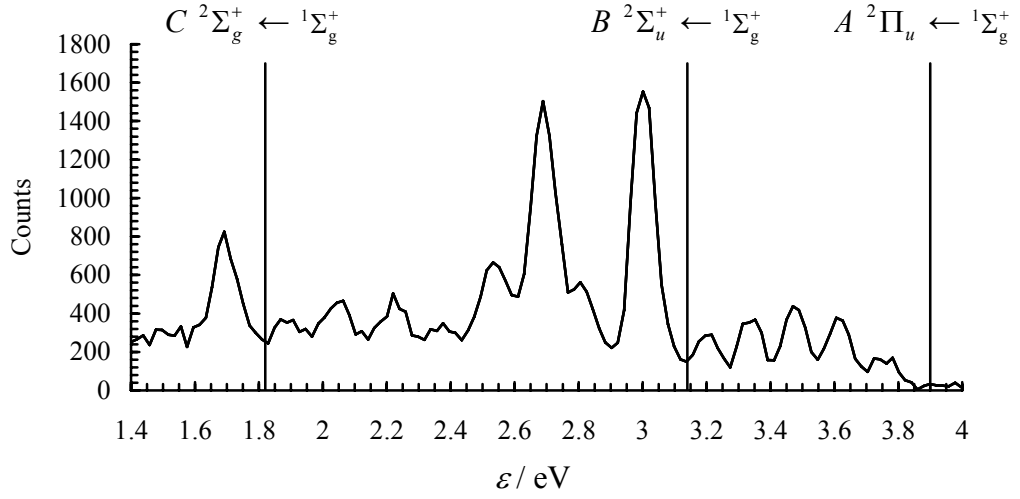

Figure 6: Ne*(40 °C) + CO_2 + HeI calibration. The vertical lines indicate the literature peak positions for the PES adiabatic transitions for the *A*, *B*, and *C* states of CO_2^+. Our peaks for these transitions are red-shifted by 0.14 eV. See the text. The accepted values for the adiabatic transitions are given by subtracting the values in Table 2 from 21.21804 eV.

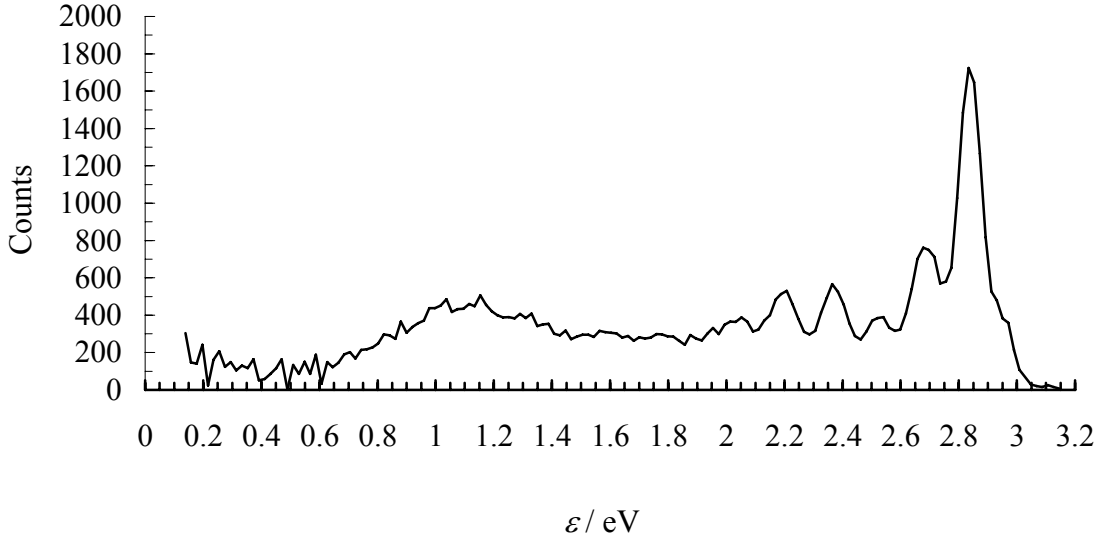

Figure 7: Energy corrected Ne*(40 °C) + CO_2 PIES spectrum. ε is the kinetic energy of the ejected electrons.

electronic ground state, simplifying matters slightly. Previously, Cermak[36] and Lescop *et al.*[4] proposed that the vibrational progressions present in the spectra of Figure 8 are the nv_1 and $nv_1 + 2v_3$ progressions. To verify this, note (Table 1) that the excitation energy for Ne* ($2p^5 3s\ ^3P_2$) is 16.6191 eV. The largest peak in the Ne* + CO_2 spectrum, therefore, should appear at (16.6191 − 13.7772) eV = 2.8419 eV, using data from Table 2. The additional peak positions in the $^3P_2$ (n00) progression are then determined by noting that the v_1 vibrational levels are separated by 1244.3 cm^{-1} = 0.15427 eV[37], yielding additional peaks at (υ = 1 to 6) 2.6876, 2.5334, 2.3791, 2.2248, and 2.0706 eV. These values neglect anharmonicity and assume that the harmonic oscillator approximation is valid, that is, $E_\upsilon = hc\,\overline{\nu}_1\,(\upsilon + ½)$. The overstrike on v_1 stresses that vibrational frequencies (e.g., v_1, v_2, etc.) that we find in tables are in units of cm^{-1}. It is convention, however, to omit the overstrike when we say, for example, that v_1 of CO_2 is 1244.3 cm^{-1}. It should be clear from context what is meant by the symbol. The shoulder on the right of the largest peak is assigned to ionization due to Ne*($2p^5 3s\ ^3P_0$), with excitation energy 16.7154 eV. Thus, the first peak in the $^3P_0$ (n00) progression should appear at (16.7154 − 13.7772) eV = 2.9382 eV, and the additional peaks in the progression should appear at 2.7839, 2.6297, 2.4754, 2.3211, and 2.1669 eV. These progressions are shown in Figure 9 in typical "pitchfork" fashion. Even with this cursory examination of peak assignments, there is no doubt that the two largest peaks are due to the $\upsilon' = 0 \leftarrow \upsilon = 0$ and $\upsilon' = 1 \leftarrow \upsilon = 0$ $^3P_2$ (n00) and the $\upsilon' = 0 \leftarrow \upsilon = 0$, $\upsilon' = 1 \leftarrow \upsilon = 0$, and $\upsilon' = 2 \leftarrow \upsilon = 0$ $^3P_0$ (n00) progressions for ionization into the $X\,^2\Pi_g$ state of CO_2^+. Such a result is, evidently, typical for linear triatomics, as the Vecchiocattivi result[12] for the PIES spectrum for Ne* + N_2O bears a resemblance to the PIES spectrum for Ne* + CO_2. The spectrum that they show, however, for Ne* + $N_2O(^3P_{2,0})$ contains no signal below 3.25 eV and only indicates peaks for the N_2O^+ $X\,^2\Pi$ vibrational progression for υ = 0, 1, and 2.

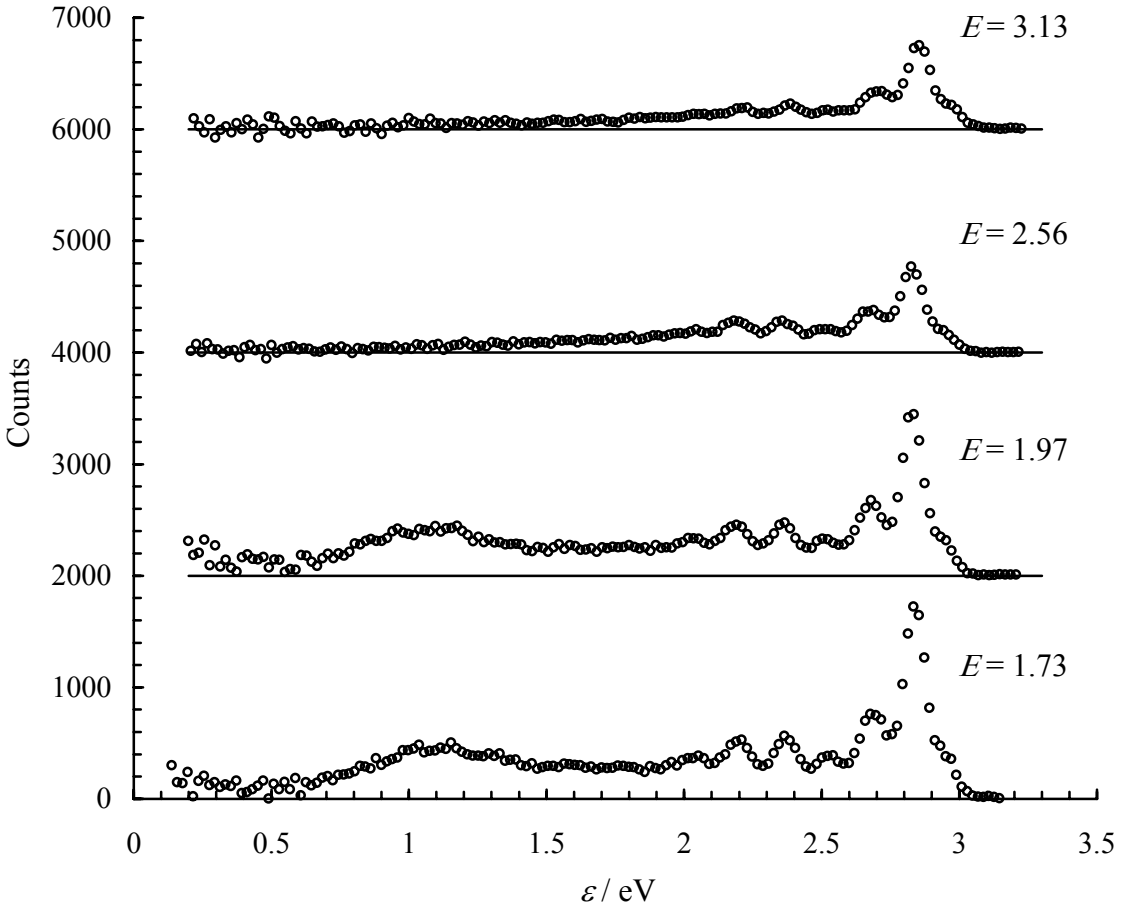

Figure 8: Energy corrected PIES spectra for Ne* + CO_2 at four collision energies. ε is the kinetic energy of the ejected electrons. The collision energies are in kcal/mol. Each circle represents the sum of the counts at each kinetic energy. The data points are separated by 0.0195 eV. The spectra have been normalized to the same peak intensity and their baselines shifted for display. E is the collision energy in kcal/mol.

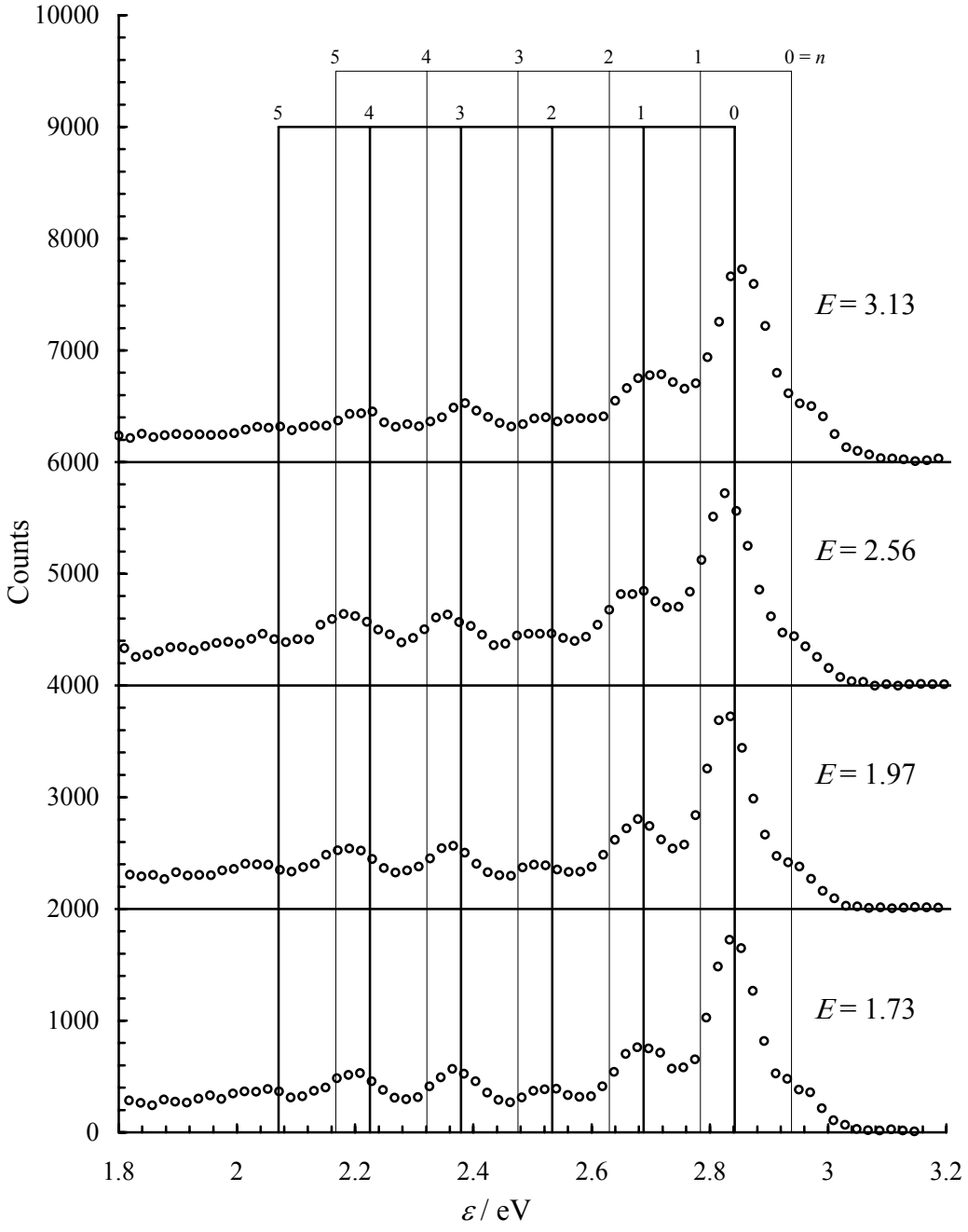

Figure 9: Energy corrected PIES spectra for Ne* + CO_2 at four collision energies. Each circle represents the sum of the counts at each kinetic energy. The data points are separated by 0.0195 eV. The spectra have been normalized to the same peak intensity and their baselines shifted for display. *E* is the collision energy in kcal/mol. The dark pitchfork shows the location of the $^3P_2$ (*n*00) progression, based on PES data in Tables 1 and 2. The light pitchfork shows the location of the $^3P_0$ (*n*00) progression, based on PES data in Tables 1 and 2. The shift of the peaks relative to these values gives us dynamical information about the Ne* + CO_2 reaction. See the text.

The assignment of the $nv_1 + 2v_3$ vibrational progressions ($^3P_2$ (n02) and $^3P_0$ (n02)) is certainly less intuitively obvious, but the pitchfork diagram of Figure 10 qualitatively confirms this assignment. Without determining the actual populations (see the Conclusions section), however, this assignment has by no means been proven conclusively in this thesis. It is certainly possible to concoct additional progressions that will appear to fit the PIES spectrum. To be quantitative, note that the v_3 vibrational levels are separated by 1423.08 cm^{-1} = 0.17644 eV [30]. It was shown above that the first peak in the $^3P_2$ v_1 progression should appear at 2.8419 eV. Thus, the first peak in the $^3P_2$ $nv_1 + 2v_3$ vibrational progression should appear at [2.8419 − 2(0.17644)]eV = 2.4890 eV. The spacing continues in units of 0.15427 eV, yielding peak positions of 2.3347, 2.1805, 2.0262 eV. Likewise, it was shown above that the first peak in the $^3P_0$ v_1 progression should appear at 2.9382 eV. Thus, the first peak in the $^3P_0$ $nv_1 + 2v_3$ vibrational progression should appear at [2.9382 − 2(0.17644)]eV = 2.5853 eV. The spacing continues in units of 0.15427 eV, yielding peak positions of 2.4311, 2.2768, and 2.1225 eV.

The Conclusions section of this thesis discusses the more complex data analysis that needs to be done on this data, but some initial findings are still possible. Within "eyeball" statistical averaging, the reactions at 1.73, 1.97, and 2.56 eV shown in Figure 9 are very similar with respect to peak position and peak shape. For each of these energies, the maximum of the most intense peak, the $v' = 0 \leftarrow v = 0$ transition for the $^3P_2$ (n00) progression, occurs at $\varepsilon(R_i)$'s that are only slightly less than ε_0. We now define the PIES shift $\Delta\varepsilon$ in our experiments: $\Delta\varepsilon = \varepsilon_{peak} - \varepsilon_0$. ε_{peak} is the electron energy at the maximum of a peak for a particular transition. For the $v' = 0 \leftarrow v = 0$ transition for Ne* + CO_2, $\Delta\varepsilon \approx -18$ meV. Thus, whatever the exact value of the shift, it is small. Note further the broad peakshape for the $v' = 0 \leftarrow v = 0$ transition with

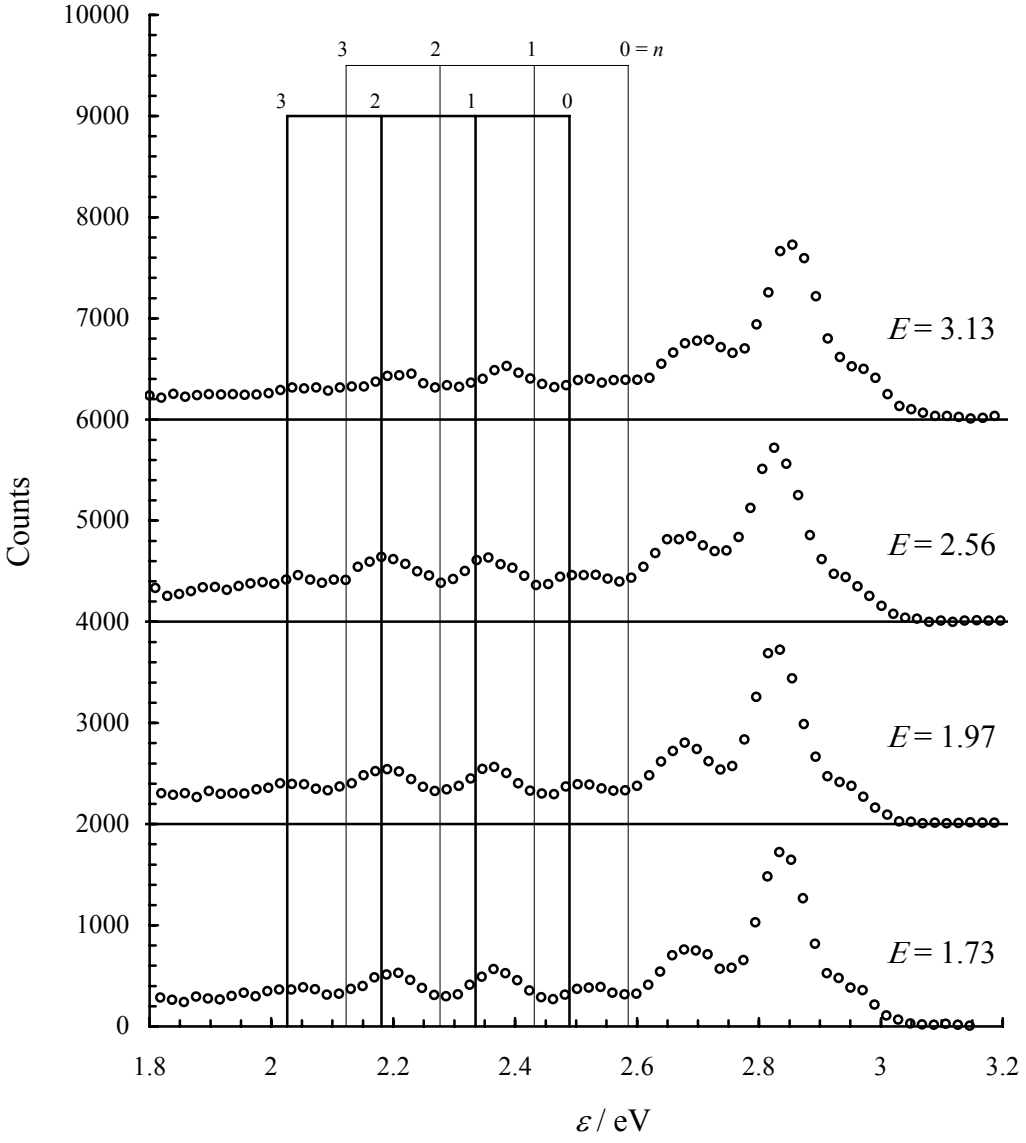

Figure 10: Energy corrected PIES spectra for Ne* + CO_2 at four collision energies. Each circle represents the sum of the counts at each kinetic energy. The data points are separated by 0.0195 eV. The spectra have been normalized to the same peak intensity and their baselines shifted for display. *E* is the collision energy in kcal/mol. The dark pitchfork shows the location of the $^3P_2$ (*n*02) progression, based on PES data in Tables 1 and 2. The light pitchfork shows the location of the $^3P_0$ (*n*02) progression, based on PES data in Tables 1 and 2.

FWHM ≈ 0.1 eV, which is significantly larger than the shift. This small shift and relatively large FWHM indicates that the electron ejection occurs very near the crossing point of V_0, that is, over geometries that occur at positive and negative regions of V_0. Our initial finding of a red shift must be contrasted with the blue shift of 16 ± 2 meV for the same transition reported by Lescop *et al*.[4] for a collision energy E of 56 meV = 1.3 kcal/mol. This E is below what we measured, and it is possible that changing collision dynamics, such as transition state geometry, could alter $\Delta\varepsilon$ between 1.3 kcal/mol and 1.73 kcal/mol. Our reaction for which E = 3.13 kcal/mol differs in peak position from the other three reactions with $\Delta\varepsilon \approx 18$ meV. If this slight blue shift is true, ionization for the E = 3.13 kcal/mol reaction must occur at significantly shorter R and, therefore, at a more repulsive region of the V_0 curve. (In this qualitative treatment, we are ignoring the complexity of potential *surfaces* (not one dimensional curves), which are the true representation for Penning ionization of *molecules*.) This, coupled with the Lescop *et al*. result, would mean that the Ne* + CO_2 reaction alternates between blue, red, and blue shifts. We are, at present, a bit skeptical of such chameleon-like behavior, and look forward to proper peak fitting to test our results more fully. (Lescop *et al*. also reported a blue shift of 22 ± 2 meV for the $^3P_0$ (100) ← (000) transition. Since the $^3P_{2,0}$ peaks were not resolved in this thesis, however, we can't compare our value to theirs.)

Next, we repeat the energy correction for the Ne* + C_2H_2 spectra. Note first Figure 11, the raw spectrum for the Ne*(40 °C) + C_2H_2 PIES experiment that was run in conjunction with the HeI + C_2H_2 PES. The calibration, however, is not as simple as the case for CO_2 for two major reasons. First, the A state PES (calibration) peaks and the PIES peaks overlap in the ε = 4.5 − 5 eV region. Second, and more importantly, even the C_2H_2 PES spectrum by itself (i.e., no

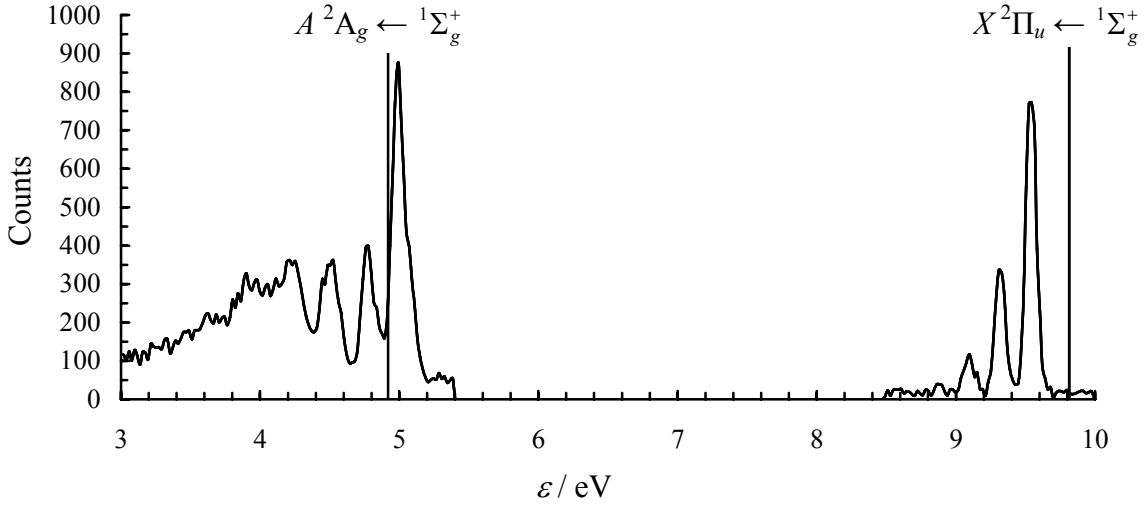

Figure 11: Ne*(40°C) + C_2H_2 + HeI calibration. The vertical lines indicate the literature peak positions for the PES adiabatic transitions for the *X* and *A* states of $C_2H_2^+$. The accepted values for the adiabatic transitions are given by subtracting the values in Table 2 from 21.21804 eV. Only the *X* state can be resolved for calibration purposes. See the text. (In some cases, for convenience, the notation $A\ ^2\Sigma_g^+ \leftarrow\ ^1\Sigma_g^+$ has been used, but this is only true for $D_{\infty h}$ symmetry, which the *A* state ion does not possess.[35])

simultaneous PIES experiment) is not resolved well enough with our data to accurately determine the adiabatic peak for the *A* state, evidenced by comparison of our spectra with the high resolution spectra that have been obtained by Ruett *et al.*[38] and Avaldi *et al.*[24]. The adiabatic transition value that is given in these papers occurs weakly due to very poor Franck-Condon overlap, which is likely the result of a significant rearrangement from linear to bent geometry in the *A* state. For this reason, only the $v' = 0$ value for the *X* state in Figure 11 will be used to deduce the needed energy correction. The raw data indicates ejected electrons of 9.53 eV for the *X* state adiabatic transition. The actual value is 9.815, obtained by subtracting the ionization potential of the $1\pi_u$ orbital (Table 2) from 21.21804 eV. Therefore, 0.29 eV must be added to the raw data kinetic energy for the Ne*(40 °C) + C_2H_2 experiment. (In the past, we have found that the change in the shift of our PES peaks from the actual values differs by no more than 0.04 eV over the range of ~10 eV. For example, whereas the adiabatic *X* peak differed from the actual value by 0.29 eV, the shift of the adiabatic *A* peak might be 0.25 eV. Since we can't prove this, we will simply use the 0.29 eV shift, a value we actually *can* prove.) The analogous correction for the two higher *E* experiments indicates that 0.26 eV must be added to the raw data kinetic energies. See Figure 12 for the energy corrected spectrum of the Ne*(40 °C) + C_2H_2 experiments. The maximum at low energy appears at 0.08 eV, narrowly reaching the positive kinetic energy range. More on this below.

The pitchfork diagram for C_2H_2 is given in Figure 13 in which the ejected electron energies have been corrected as described above. Note, however, that only the *X* state is shown. The previous work of B. Lescop *et al.*[7] on Ne* + C_2H_2 likewise did not include a presentation of the *A* state. We are justified in this because, while it is true that interaction between the

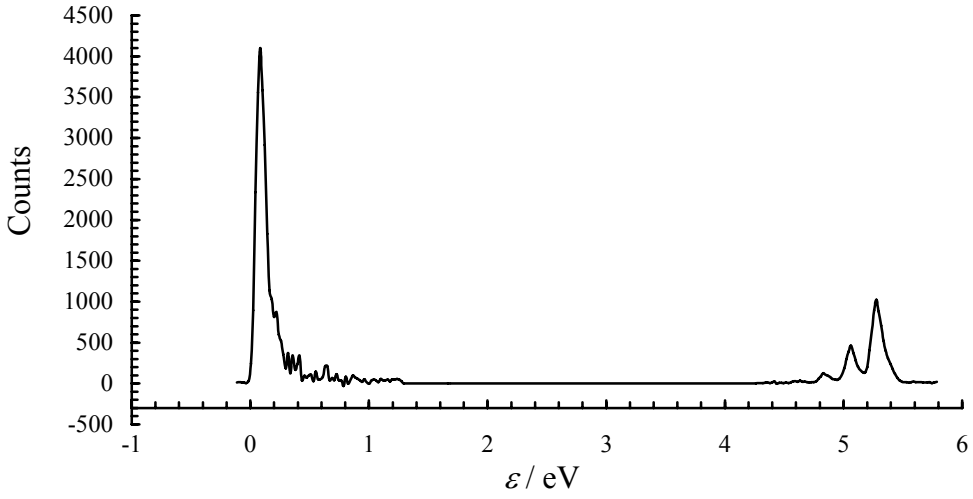

Figure 12: Energy corrected Ne*(40 °C) + C_2H_2 PIES spectrum. ε is the kinetic energy of the ejected electrons. No data were collected in the middle energy region.

reactants in a PI reaction shifts peaks somewhat and intensities (i.e., populations) vary, the peak position for the low energy peak is shifted impossibly far from a reasonable value. The difference between the *A* state adiabatic ionization energy for C_2H_2 and Ne*($^3P_2$) is 0.322 eV. (See Tables 1 and 2.) A peak at 0.08 eV, as we have in Figure 12, would mean that the interaction of the colliding Ne* and C_2H_2 was so great that it induced a shift of roughly 0.24 eV for the *A* state − a shift that is much too large. Further, we have already discussed, in part, the complex PES spectrum for the *A* state of C_2H_2. Resolving a *good* PIES spectrum for this state would be difficult, but we evidently do not even have a good *A* state PIES peak. The exact meaning of the low energy peak in Figure 12 is certainly a question that needs further exploration. (It may indicate a limitation of our apparatus.) We do know, however, that it *is* PIES signal, because, for example, the Ne* + CO_2 reaction produces no such peak; Penning spectra are very "quiet". The very soft ionization due to the closeness of the energies of Ne* ($^3P_2$) and the *IE* of the $3\sigma_g$ MO of C_2H_2, perhaps, plays a significant role.

To determine our pitchforks for Figure 13, note that Tables 1 and 2 give ε_0 = 5.216 eV for the adiabatic transition into the $X\,C_2H_2^+$ electronic state for reaction with Ne* $^3P_2$. For Ne* $^3P_0$, the analogous value is 5.312 eV. Now, the well resolved peaks for the X state PIES spectrum of $C_2H_2^+$ imply a simple progression. (The situation with CO_2 is *much* more complicated, evidenced by the broad band of signal in its PIES spectrum. Note that the peak assignments that were attempted for CO_2 above were only for energies above ~2 eV, whereas there is signal down to at least 0.5 eV.) The energy spacing between the peaks at ~5 eV in the PIES spectrum for all three Ne* + C_2H_2 collision energies (see Figure 13) is 0.23 ± 0.01 eV, using, again, "eyeball" statistical averaging. υ_2 in $C_2H_2^+$ (the CC stretch) is[39] 1829 cm^{-1} = 0.2268 eV, agreeing very nicely with our data, if there is only the υ_2 progression present. Thus, the spacing between the peaks due to the $^3P_{2,0}$ progressions are determined by simply subtracting units of 0.23 eV from 5.216 and 5.312 eV, respectively.

Increasing blue shift and concomitant peak broadening are consistent with transitions that occur over a predominantly repulsive excited-state potential energy curve, a result seen in previous work for Ne* + H_2.[17] Our results for C_2H_2, as seen in Figure 13, however, are mixed. All of the spectra have a sizable blue shift ($\Delta\varepsilon > 0$), indicating that electron ejection occurs primarily on the repulsive part of V_0, as described above, but the blue shift *decreases* with increasing E. (We must be cautious in our red or blue shift preliminary findings for both CO_2 and C_2H_2 because the energy correction that was used in this thesis was not done in as detailed a manner as possible. See the Conclusions section for a discussion of this.) To explain *increasing* blue shift as E increases, refer to Figure 2. As E increases, the reactants are able to approach more closely, that is, reach smaller R values, before reaction occurs. Therefore, they are higher

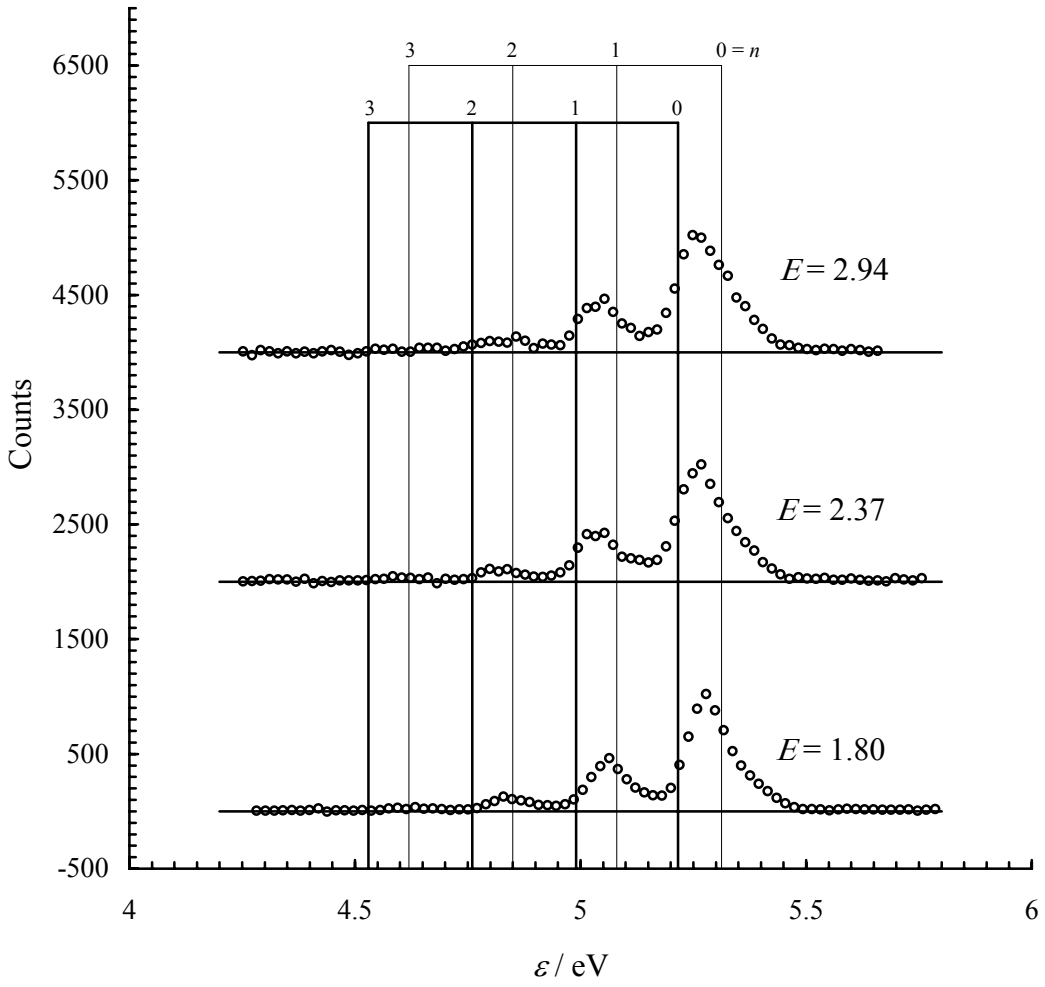

Figure 13: Energy-corrected *X* state spectra for the PIES Ne* + C_2H_2 reaction at three collision energies. Each circle represents the sum of the counts at each kinetic energy. The data points are separated by 0.0195 eV. The spectra have been normalized to the same peak intensity and their baselines shifted for display. *E* is the collision energy in kcal/mol. The dark pitchfork indicates the $^3P_2$ (0*n*000) progression, based on PES data in Tables 1 and 2. The light pitchfork indicates the $^3P_0$ (0*n*000) progression, based on PES data in Tables 1 and 2**.**

up on the repulsive part of V_0 when the transition occurs, leading to larger blue shifts. That we get *decreasing* blue shift with increasing E is not typical and could be due to changing dynamic factors as E increases, or the data could simply be poor. A survey of the literature produced no other kinetic energy of collision tests for Ne* + C_2H_2, so we don't have another group's work with which to compare our result. Lescop *et al*.[7] did conduct Ne* + C_2H_2 at an unspecified E and found a blue shift of $\Delta\varepsilon = 25 \pm 4$ meV for the $^3P_2$ (01000) ← (00000) transition and $\Delta\varepsilon = 30 \pm 4$ meV for the $^3P_0$ (01000) ← (00000) transition. The estimate for our experiment of this same transition is $\Delta\varepsilon = 60$, 50, and 45 meV for the three kinetic energies tested, respectively. Our dramatic blue shift agrees with the Lescop *et al*. result in part. Further, the increase in magnitude over the shift observed for CO_2 that Lescop *et al*. found was duplicated by our group, as well. Figure 13 also shows that there is peak broadening as E increases. For the $v' = 0 \leftarrow v = 0$ transitions FWHM ≈ 0.1 eV for $E = 1.80$ kcal/mol and FWHM ≈ 0.12 eV for $E = 2.94$ kcal/mol. Peak broadening is chiefly the result of the sharp increase in $\Gamma(R)$ at short R. $\Gamma(R)$ is an "enabler" for the reaction, and, as described above, it is quantum mechanical. Thus, as $\Gamma(R)$ grows, the range of R values over which the *same transition* can occur increases, and the peak broadens. A minor contributing factor to peak broadening is that the velocity distribution in our beam increases as E increases. See above. (This explanation implies that we should never see a red shift and peak broadening. If anything, the peaks might become more narrow.)

4.0 CONCLUSIONS

This thesis is a preliminary investigation of Ne* + CO_2 and Ne* + C_2H_2 PIES reactions. The information gathered here will be used to conduct further investigations in the laboratory and to guide additional analysis of the data. We semiquantitatively agree with the assignment of nv_1 and $nv_1 + 2v_3$ progressions to the Ne* + CO_2 PIES spectra that has been offered by Cermak[36] and B. Lescop *et al*.[4]. It is not transparent, however, from either of these articles that other progressions have been considered. The Cermak paper, in fact, explicitly uses the word "tentative" to describe the assignments. The nv_1 is beyond doubt, but the $nv_1 + 2v_3$ progression should be tested against other possible progressions once peak fitting has been performed and populations of the vibrational levels have been determined. Note, however, that $\Delta v_3 = \pm 2$ is a selection rule for the antisymmetric stretch for any molecule with $D_{\infty h}$ symmetry, which serves as a basis for suggesting that this progression is present. Note that the v_2 mode is not considered due to the fact that removal of the electron from the $1\pi_g$ MO, which is largely localized on the O atoms, apparently does not produce a significant change in geometry. A geometry (more correctly, symmetry) change upon ionization is as important as the energy (frequency) of a vibration for determining whether the ionization will lead to excitation of the normal mode. Note further that v_2 is, in fact, the *lowest* energy vibration for CO_2^+, indicating that the energy of vibration, even if it is low, is certainly not the only factor that determines excitation. A slight red shift was found for the three lowest E's tested for CO_2. We found a blue shift for the highest E

for CO_2. v_1 and $v_1 + 2v_3$ progressions were qualitatively confirmed for the CO_2 PIES spectra. A blue shift, greater in magnitude than the shift we found in CO_2, was found for all E's tested for Ne* + C_2H_2. The X state of the PIES spectrum for Ne* + C_2H_2 was resolved as a simple progression of the v_2 C−C stretch. The A state suffers from appearing at the threshold for Ne*($^3P_2$) and near threshold for Ne*($^3P_0$) as well as the excitation of several vibrational progressions and non Franck-Condon behavior. The energy correction that we used above was achieved by "eyeball" statistics on the PES peaks of spectra such as those presented in Figures 6 and 11. This can be improved by peak fitting and must be as accurate as possible since the PES-indicated energy correction to the raw data was between 0.14 − 0.29 eV, a value that is much larger than the red shift ($\Delta\varepsilon \approx -18$ meV) for CO_2 and the blue shift for C_2H_2 ($\Delta\varepsilon \approx 50$ meV). The FWHM was roughly 0.1 eV for both reactions, indicating, as described above, that the ionization on the respective V_0 surfaces in both reactions occurs over a range of R values of similar magnitude. (The range has the same magnitude, not necessarily equal R's.) The significantly greater magnitude of $\Delta\varepsilon$ in the case of C_2H_2 indicates, however, that the ionization for Ne* + C_2H_2 occurs over a greater segment of the positive part of V_0 than does the ionization seen in Ne* + CO_2. The smaller overall shift plus broad peakshapes and the move from red shifts at lower E's to a blue shift at the highest E for the ionization in Ne* + CO_2 can be explained by ionization that occurs near the crossing point of V_0.

The peak fitting procedure begins with a rather difficult transmission correction which attempts to account for the fact that the einzel lens is more successful at capturing slow electrons than fast ones. Briefly, PES of N_2, CO, and O_2 spectra are obtained at the prevailing set of experimental conditions at which the PIES experiments were performed. Since the relative peak

intensities of N_2, CO, and O_2 PES spectra have been *very* well documented, comparison of what our PES peak ratios are to the actual ratios indicates how well or poorly our instrument is transmitting electrons at various energies in current experiments. Often the analyzer yields peak heights (counts) at low kinetic energy that are too large and peak heights at high kinetic energy that are too small, and we try to find the best-fit, linear (if possible) correction that shrinks the low kinetic energy peaks and enhances the high kinetic energy peaks. Further peak fitting involves use of a FORTRAN program, authored by the redoubtable P. E. Siska, called gelspec.for that fits the peaks, after an initial guess, to Gaussians through a gradient expansion least squares calculation. This program is easily run on any desktop computer in seconds. To obtain the final fit, we use populations from the raw data to "guide" the program as it seeks the best fit curve, while parameters are varied that fit peak widths (FWHM) for the PES and PIES peaks, the PES energy shift, and the $^3P_{2,0}$ peak ratio for the Ne* metastable. This process is described more fully in reference [17].

It should also be pointed out that our PES peaks do not resolve the spin-orbit splitting in, for example, the *A* state of CO_2, yet we used the adiabatic value (17.3132 eV) in the course of determining the energy calibration. This produces a very small error, however, since the $J = 3/2$ and $J = 1/2$ states are separated by a mere 0.0118 eV. Additionally, the experience with C_2H_2 was quite useful. In the future the PES/PIES calibration run for Ne* + C_2H_2 should probably be performed with a seed gas, as described above, since the PIES and PES peaks overlap around 5 eV and since the *A* state PES for C_2H_2 is so complex. Even using the most well resolved peak of the PES *A* state to calibrate the instrument for C_2H_2 PIES experiments is problematic because it is actually a doublet, when properly resolved, split by about 0.08 eV.[24] An alternative is to

resolve this *A* state doublet through peak fitting the PES data. While these might seem like tiny energy corrections to consider, consider the small size of the shift from our preliminary observations for Ne* + CO_2. To verify that these shifts are actually there or are, in fact, statistically insignificant, will require that the calibration be as exact as possible.

APPENDIX

Below we outline how to calculate the initial energy of the system E, as defined previously, at a particular nozzle temperature. Analysis of supersonic jets[40,41] leads to the main conclusion that the beam of gas that emerges from a very small orifice is "cold" in the sense that it has a very narrow velocity distribution. The gas particles' flow velocity v_f, the velocity relative to the reference frame of the laboratory, is nonetheless typical in magnitude of any gas as described by the Maxwell-Boltzmann velocity distribution. (The velocity distribution is, however, certainly *not* Maxwellian.) For supersonic jets v_f is given by a modified version of the Maxwell-Boltzmann most probable velocity formula:

$$v_f = \sqrt{\frac{\gamma}{\gamma - 1}} \sqrt{\frac{2k_B(T_0 - T)}{m}} . \qquad (4)$$

γ is the heat capacity ratio C_P/C_V, T_0 is the temperature of the nozzle, T is the cooled translational temperature, and m is the mass of a single gas atom or molecule. γ has the approximate value of 5/3 for ideal monatomic gases (e.g., He and Ne) or 7/5 for diatomic rigid rotors (e.g., N_2 and H_2) and other linear polyatomic molecules (e.g., CO_2 and C_2H_2) with no low frequency vibrations. For nonlinear polyatomic molecules $\gamma = 4/3$. These approximate values come from the equipartition theorem. The value of 5/3 is nearly exact for the noble gases, and we use it for neon. The more exact value for CO_2 that has been obtained for our spectrometer[42]

is 1.395 and will be used here. Since energy can be stored in the internal (rotational and vibrational) degrees of freedom, thereby affecting the heat capacities, it is important to point out that the large number of collisions that occur in the nozzle relax the rotations and vibrations of the molecule, converting rotational and vibrational energy into translational energy. Usually, most vibrational levels are not occupied, and little energy is stored in them. The energy in rotation, however, is significant, sometimes resulting in *heavier* particles having a *greater* v_f, than lighter particles, once the rotational energy has been converted to translational motion. Such is that case here, where C_2H_2 has a greater v_f than Ne. We make the assumption, then, that C_2H_2 has no occupied vibrational levels and no low frequency vibrations that can become excited. Thus, we use $\gamma = 7/5$ for C_2H_2. (Note, also, that any residual vibrational energy does not contribute to the translational velocity of the gas.)

In Equation 4 T is a measure of the velocity spread in the beam; the lower T is, the smaller the spread in velocity. To determine T, we first need S, the speed ratio, given by

$$S = M\sqrt{\frac{\gamma}{2}}, \tag{5}$$

where M is the mach number, the ratio of v_f to the local speed of sound. It is no simple task to determine M, which can be obtained by time of flight analysis.[43] Here, we use $M(CO_2) = 8.4$, as determined in the referenced time of flight measurements. Further, we estimate that $M(Ne) = 15$ and $M(C_2H_2) = 8$. T is then given by

$$T = \frac{T_0}{1 + \left(\frac{\gamma - 1}{\gamma}\right) S^2}. \tag{6}$$

Note that for infinite M, T = 0, reducing the second factor of Equation 4 to the exact formula for the most probable velocity of a gas in a Maxwellian distribution. Thus, any nonzero T works to *decrease* v_f relative to the most probable velocity of a gas in a Maxwellian beam. M increases lead to smaller T values, via Equations 5 and 6, and M can vary significantly between seemingly similar molecules. The first factor of Equation 4, however, is always greater than 1, which works to *increase* v_f relative to the most probable velocity of a gas in a Maxwellian beam. Thus, the correlation between v_f, m, and M can't be simply stated, nor can the values of v_f for two different molecules be easily predicted. As noted above, C_2H_2 has a *larger* v_f than Ne. CO_2, however, has a smaller v_f than Ne. The T correction, generally, is small, and the first factor in Equation 4 ensures that v_f for a supersonic beam of gas always exceeds the most probable velocity for a Maxwellian beam.

Now v_f can be calculated. To be slightly more accurate, however, it is better to use the most probable velocity v_{mp} to determine E via Equation 1. v_{mp} is given by

$$v_{mp} = v_f \left(1 + \frac{1}{S^2}\right). \tag{7}$$

As shown in Figure 1, we calculate v_{rel} by the Pythagorean Theorem, giving

$$v_{\text{rel}}^2 = \left(v_{\text{mp}}^{\text{Ne*}}\right)^2 + \left(v_{\text{mp}}^{\text{CO}_2}\right)^2. \tag{8}$$

Finally, then, the collision energy is given by substituting into Equation 1:

$$E = \frac{1}{2}\mu v_{\text{rel}}^2 = \frac{1}{2}\mu\left[\left(v_{\text{mp}}^{\text{Ne*}}\right)^2 + \left(v_{\text{mp}}^{\text{CO}_2}\right)^2\right]. \tag{9}$$

Next, we complete the actual calculation for Ne* + CO_2, leaving T_0 so that we can calculate E at the four different nozzle temperatures used. Combining Equations 5 and 6 for Ne gives

$$T = \frac{T_0}{1+\frac{1}{2}(\gamma-1)M^2} = \frac{T_0}{1+\frac{1}{2}\left[\left(\frac{5}{3}\right)-1\right](15)^2} = \frac{T_0}{76}. \tag{10}$$

Next, the flow velocity is given by

$$\begin{aligned} v_{\text{f}}^{\text{Ne*}} &= \sqrt{\frac{\gamma}{\gamma-1}}\sqrt{\frac{2k_{\text{B}}(T_0-T)}{m}} \\ &= \sqrt{\frac{5/3}{\frac{5}{3}-1}} \times \sqrt{\frac{2(1.38065 \times 10^{-23}\ \text{J/K})\left(T_0 - \frac{T_0}{76}\right)}{20.1797\ \text{amu}\left(\frac{1.66054 \times 10^{-27}\ \text{kg}}{1\ \text{amu}}\right)}} \\ &= 45.38839\ \text{m s}^{-1}\ \text{K}^{-1/2}\sqrt{T_0 - \frac{T_0}{76}} = 45.08879\ \text{m s}^{-1}\ \text{K}^{-1/2}\sqrt{T_0} \end{aligned}. \tag{11}$$

The most probable velocity follows from

$$v_{\mathrm{mp}}^{\mathrm{Ne*}} = v_{\mathrm{f}}^{\mathrm{Ne*}}\left(1+\frac{1}{S^2}\right) = 45.08879\ \mathrm{m\ s^{-1}\ K^{-1/2}}\sqrt{T_0}\ \times \left(1+\frac{1}{M^2\left(\frac{\gamma}{2}\right)}\right)$$

$$= 45.08879\ \mathrm{m\ s^{-1}\ K^{-1/2}}\sqrt{T_0}\ \times \left(1+\frac{1}{(15)^2\left(\frac{5/3}{2}\right)}\right) \quad . \tag{12}$$

$$= 45.32926\ \mathrm{m\ s^{-1}\ K^{-1/2}}\sqrt{T_0}$$

For CO_2 $T_0 = 313$ K for all of the reactions that were run. Thus, combining Equations 5 and 6 gives

$$T = \frac{T_0}{1+\frac{1}{2}(\gamma-1)M^2} = \frac{313\ \mathrm{K}}{1+\frac{1}{2}(1.395-1)(8.4)^2} = 20.95664\ \mathrm{K}\ . \tag{13}$$

The flow velocity is given by

$$v_{\mathrm{f}}^{\mathrm{CO_2}} = \sqrt{\frac{\gamma}{\gamma-1}}\sqrt{\frac{2k_{\mathrm{B}}(T_0-T)}{m}}$$

$$= \sqrt{\frac{1.395}{1.395-1}}\ \times \sqrt{\frac{2(1.38065\ \times\ 10^{-23}\ \mathrm{J/K})(313\ \mathrm{K}-20.95664\ \mathrm{K})}{44.010\ \mathrm{amu}\left(\frac{1.66054\ \times\ 10^{-27}\ \mathrm{kg}}{1\ \mathrm{amu}}\right)}} \tag{14}$$

$$= 624.23967\ \mathrm{m\ s^{-1}}$$

The most probable velocity is given by

$$
\begin{aligned}
v_{\mathrm{mp}}^{\mathrm{CO_2}} &= v_{\mathrm{f}}^{\mathrm{CO_2}}\left(1+\frac{1}{S^2}\right) = 624.23967\ \mathrm{m\ s^{-1}} \times \left(1+\frac{1}{M^2\left(\frac{\gamma}{2}\right)}\right) \\
&= 624.23967\ \mathrm{m\ s^{-1}} \times \left(1+\frac{1}{(8.4)^2\left(\frac{1.395}{2}\right)}\right) \\
&= 636.92345\ \mathrm{m\ s^{-1}}
\end{aligned}
\tag{15}
$$

Now that we have v_{mp} for both reactants, E is given by Equation 1:

$$
\begin{aligned}
E &= \frac{1}{2}\mu v_{\mathrm{rel}} = \frac{1}{2}\mu\left[\left(v_{\mathrm{mp}}^{\mathrm{Ne^*}}\right)^2+\left(v_{\mathrm{mp}}^{\mathrm{CO_2}}\right)^2\right] \\
&= \frac{1}{2}\left(\frac{44.010\ \mathrm{amu}(20.1797\ \mathrm{amu})}{64.190\ \mathrm{amu}}\right)\left(\frac{1.66054\times10^{-27}\ \mathrm{kg}}{1\ \mathrm{amu}}\right) \\
&\quad\times\left[\left(45.32926\ \mathrm{m\ s^{-1}\ K^{-1/2}}\sqrt{T_0}\right)^2+\left(636.92345\ \mathrm{m\ s^{-1}}\right)^2\right] \\
&= 1.14873\times10^{-26}\ \mathrm{kg}\left[2054.742\ \mathrm{m^2\ s^{-2}\ K^{-1/2}}(T_0)+405671\ \mathrm{m^2\ s^{-2}}\right]
\end{aligned}
\tag{16}
$$

Finally, we have a general equation that simply requires input of T_0 in K for Ne*. The above formula is in SI units and gives E in units of J/collision. This is easily converted to the kcal/mol values that are given in the Results section of this thesis. Repeating this process for C_2H_2 generates the following general formula:

$$
\begin{aligned}
E &= \frac{1}{2}\mu v_{\text{rel}}^2 = \frac{1}{2}\mu\left[\left(v_{\text{mp}}^{\text{Ne*}}\right)^2 + \left(v_{\text{mp}}^{\text{C}_2\text{H}_2}\right)^2\right] \\
&= \frac{1}{2}\left(\frac{26.038\ \text{amu}(20.1797\ \text{amu})}{46.218\ \text{amu}}\right)\left(\frac{1.66054\ \times\ 10^{-27}\ \text{kg}}{1\ \text{amu}}\right) \\
&\quad \times\ \left[\left(45.32926\ \text{m s}^{-1}\ \text{K}^{-1/2}\sqrt{T_0}\right)^2 + \left(823.56354\ \text{m s}^{-1}\right)^2\right] \\
&= 9.43910\ \times\ 10^{-27}\ \text{kg}\left[2054.742\ \text{m}^2\ \text{s}^{-2}\ \text{K}^{-1/2}(T_0) + 678253\ \text{m}^2\ \text{s}^{-2}\right]
\end{aligned}
\tag{17}
$$

BIBLIOGRAPHY

[1] V. Cermak, Z. Herman, Coll. Czech. Chem. Comm. **30**, 169 (1965).

[2] P. E. Siska, Rev. Mod. Phys. **65** 341-343 (1993).

[3] H. M. Bevseck, Ph.D. Thesis, University of Pittsburgh (1996).

[4] B. Lescop, M. Ben Arfa, M. Cherid, G. Le Coz, G. Sinou, G. Fanjoux, A. Le Nadan, and F. Tuffin, J. Chem. Phys. **108**, 550 (1998).

[5] R. Maruyama, H. Tanaka, Y. Yamakita, F. Misaizu, K. Ohno, Chem. Phys. Lett. **327**, 104 (2000).

[6] M. Ben Arfa, B. Lescop, M. Cherid, B. Brunetti, P. Candori, D. Malfatti, S. Falcinelli, F. Vecchiocattivi, Chem. Phys. Lett. **308**, 71 (1999).

[7] B. Lescop, M. Ben Arfa, M. Cherid, G. Le Coz, G. Sinou, G. Fanjoux, A. Le Nadan, and F. Tuffin, J. Elec. Spec. Rel. Phen. **87**, 51 (1997).

[8] A. Le Nadan,G. Sinou, and F. Tuffin, J. de Physique II **3**, 775 (1993).

[9] B. Lescop, M. Ben Arfa, M. Cherid, G. Fanjoux, E. Kassab, J. de Chimie Physique et de Physico-Chimie Biologique **95** 2113 (1998).

[10] B. Lescop, M. Ben Arfa, G. Le Coz, M. Cherid, G. Sinou, A. Le Nadan, and F. Tuffin, Chem. Phys. Lett. **252**, 327 (1996).

[11] A. Aguilar, B. Brunetti, M. Gonzalez, and F. Vecchiocattivi, Chemical Physics **145**, 211 (1990).

[12] F. Biondini, B. Brunetti, P. Candori, F. De Angelis, S. Falcinelli, F. Tarantelli, M. Teixidor, F. Pirani, F. Vecchiocattivi, J Chem. Phys. **122**, 164307 (2005).

[13] F. Biondini, B. Brunetti, P. Candori, F. De Angelis, S. Falcinelli, F. Tarantelli, M. Teixidor, F. Pirani, F. Vecchiocattivi, J Chem. Phys. **122**, 164308 (2005).

[14] H. M. Bevsek, D. C. Dunlavy, P. E. Siska, J. Chem. Phys. **102**, 133 (1995).

[15] D. C. Dunlavy, P.E. Siska, J. Phys. Chem., **100**, 21 (1996).

[16] H. M. Bevsek, Ph.D. Thesis, University of Pittsburgh (1996).

[17] J. H. Noroski and P. E. Siska, J. Chem. Phys. **125**, 133118/9 (2006).

[18] J. Noroski, L. Park, and P. E. Siska (unpublished).

[19] P. E. Siska, Rev. Mod. Phys. **65** 338 (1993).

[20] N. Kishimoto, E. Matsumura, K. Ohno, J. Chem. Phys. **121** (7): 3074-3086 (2004).

[21] M. Yamazaki, S. Maeda, K. Ohno K., Chem. Phys. Lett. **391** (4-6): 366-373 (2004).

[22] W. H. Miller, J. Chem. Phys. **52** 3563 (1970).

[23] A. P. Hickman and H, Morgner, J. Phys. B **9** 1765 (1976).

[24] L. Avaldi, G. Dawber, R. Hall, G. King, A. McConkey, M. MacDonald, G. Stefani, J. Elec. Spec. Rel. Phen. **71**, 93 (1995).

[25] C. Weiser and P. E. Siska, Rev. Sci. Instrum. **58**, 2124 (1987); Z. Phys. D **10**, 165 (1988).

[26] E. Harting, F. H. Read, *Electrostatic Lenses*, Elsevier: New York, (1976).

[27] J. H. Moore, C. C. Davis, and M. A. Coplan, *Building Scientific Apparatus,* Addison-Wesley: London, 1983.

[28] J. Ingle, S. Crouch, *Spectrochemical Analysis*, Prentice Hall, New Jersey, 212 (1988).

[29] *CRC Handbook of Chemistry and Physics*, 86th Ed., CRC Press, Boca Raton, 10-208 (2005).

[30] P. Baltzer, F. Chau, J. Eland, L. Karlsson, M. Lundqvist, J. Rostas, K. Tam, H. Veenhuizen, B. Wannberg, J. Chem. Phys. **104**, 8922 (1996).

[31] L. Wang, J. Ruett, Y. Lee, and D. Shirley, J. Elec. Spec. Rel. Phen. **47**, 171 (1988).

[32] R. T. Wiedmann, E. R. Grant, R. G. Tonkyn, M. G. White, J. Chem. Phys. **95**, 752 (1991).

[33] W. Kong, D. Rodgers, J. W. Hepburn, Chem. Phys. Lett. **221** 301 (1994).

[34] E. Kinmond, J. Eland, L. Karlsson, Inter. J. Mass. Spec. **185**/**186**/**187** 437 (1999).

[35] D. Holland, M. MacDonald, M. Hayes, L. Karlsson, B. Wannberg, J. Elec. Spec. Rel. Phen. **97**, 253 (1998).

[36] V. Cermak, J. Elec. Spec. Rel. Phen. **9**, 419 (1976).

[37] J. M. Frye and T. J. Sears, Mol. Phys. **62**, 919 (1987).

[38] J. Ruett, L. Wang, J. Pollard, D. Trevor, Y. Lee, D. Shirley, J. Chem. Phys. **84**, 3022 (1986).

[39] C. Baker, D. W. Turner, Proc. Roy. Soc. **A308**, 19 (1968).

[40] J. B. Anderson, R. P. Andres, and J. B. Fenn, Adv. Chem. Phys. **10** 275 (1966).

[41] H. C. W. Beijerinck and N. F. Vester, Physica **111C** 327 (1981).

[42] J. Pazun, Ph.D. Thesis, University of Pittsburgh (1991).

[43] D. C. Dunlavy and P. E. Siska, J. Phys. Chem. **100** 21 (1996); D. C. Dunlavy, Ph.D. Thesis, University of Pittsburgh (1996).